# Optimizing Thermal Comfort and Life Cycle Cost in High-Altitude Rural Housing Using NSGA-II and EnergyPlus

Enrique Mejia-Solis *, Tom Göransson, Björn Palm

Posted Date: 27 February 2026

doi: 10.20944/preprints202602.1796.v1

Keywords: thermal comfort; rural housing; EnergyPlus; NSGA-II; retrofit; building energy; energy efficiency; high-altitude

 doi:10.20944/preprints202602.1796.v1



*Article*

# Optimizing Thermal Comfort and Life Cycle Cost in High-Altitude Rural Housing Using NSGA-II and EnergyPlus

**Enrique Mejia-Solis [1,2,*], Tom Göransson [1] and Björn Palm [1]**

[1] Department of Energy Technology, KTH Royal Institute of Technology, SE-100 44 Stockholm, Sweden

[2] Grupo de Apoyo al Sector Rural, Pontificia Universidad Católica del Perú, Lima 15088, Peru

* Correspondence: enriquemejiasolis@gmail.com

**Abstract**

Improving indoor thermal comfort in high-altitude rural housing remains a persistent challenge for low-income communities in the Peruvian Andes. This study evaluates the thermal performance of a standardized Sumaq Wasi modular dwelling in Langui (Cusco, Peru, 3969 m.a.s.l.) and proposes passive envelope modifications that enhance comfort while preserving economic feasibility. A multi-objective optimization approach combining EnergyPlus simulations with the NSGA-II algorithm was applied to minimize total thermal discomfort ($TDI_{total}$), bedroom underheating ($TDIU_{bedrooms}$), and 10-year life cycle costs ($LCC$). The calibrated model incorporated field measurements of indoor air temperatures. Global sensitivity analysis using Morris and Sobol methods identified ceiling thermal transmittance as the dominant contributor for $TDI_{total}$, and exterior wall solar absorptance as the driver of $TDIU_{bedrooms}$. Optimization reduced $TDI_{total}$ and $TDIU_{bedrooms}$ to 22% and 8% of the base case, requiring additional investments of USD 2,347 and USD 1,959, above the base case cost (USD 8,100), respectively. Cost-neutral strategies, raising exterior-wall solar absorptance to 0.9 and increasing the skylight-to-roof ratio (13.1%), reduced bedroom underheating to 30% of the base case and outperformed a scenario with two 400W electric heaters. These results demonstrate that context-appropriate passive design can substantially improve comfort under severe climatic and financial constraints.

**Keywords:** thermal comfort; rural housing; EnergyPlus; NSGA-II; retrofit; building energy; energy efficiency; high-altitude

## 1. Introduction

Despite decades of public investment in housing programs, residents of high-altitude rural areas in Peru still face poor indoor thermal comfort and limited access to heating [1]. The cold indoor temperatures in these homes have been linked to adverse health outcomes and social vulnerability [2–5]. At the same time, housing policies and design guidelines often replicate construction solutions that fail to address the specific climatic and socioeconomic context of the Andean region [6,7]. This is especially critical given that a large proportion of the rural population in the Peruvian Andes resides above 3,500 m.a.s.l., where night-time temperatures during the coldest months commonly fall below 0-5°C [6,8,9]. Improving the energy performance of homes in these contexts could contribute to reducing energy poverty, improving health outcomes, and increasing social resilience, especially for vulnerable groups such as the elderly and young children [5,7,10,11]. However, there remains a lack of evidence-based guidance on cost-effective passive solutions, such as reduction of infiltration, increasing of solar gains, or passive heating methods, tailored to this setting [7,9,12,13].

Optimization strategies in building design aim to improve environmental performance and support informed decision-making through the systematic improvement of predefined building typologies and retrofit options [14–16]. Multi-objective optimization models are particularly useful

 doi:10.20944/preprints202602.1796.v1



in this context, as they allow competing objectives, such as minimizing energy use and maximizing thermal comfort, to be evaluated simultaneously [17,18]. These models enable the comparison of alternative performance improvement scenarios under predefined geometric, technical, and economic constraints [19]. Among optimization techniques, genetic algorithms (GAs), which mimic natural selection processes, are widely used due to their effectiveness in navigating complex solution spaces [19,20]. The Non-dominated Sorting Genetic Algorithm II (NSGA-II), in particular, has proven to be a robust and efficient tool for solving multi-objective problems in building energy performance optimization [15,16,21].

Passive methods remain the most cost-effective approach to enhancing thermal comfort in buildings, especially in low-income settings [16,22,23]. These strategies rely on the climatic adaptation of building geometry, materials, and envelope configurations to reduce energy demand [24,25]. In high-altitude Andean contexts, vernacular construction techniques, such as adobe walls, thermal mass floors, and compact layouts, demonstrate local knowledge of climate-responsive design [26–29]. Recent studies advocate for the integration of traditional passive techniques with modern performance evaluation tools to identify affordable and culturally appropriate retrofit strategies [7,8,30–34].Passive methods remain the most cost-effective approach to enhancing thermal comfort in buildings, especially in low-income settings [22,35]. These strategies rely on the climatic adaptation of building geometry, materials, and envelope configurations to reduce energy demand [24,36,37]. In high-altitude Andean contexts, vernacular construction techniques, such as adobe walls, thermal mass floors, and compact layouts, demonstrate local knowledge of climate-responsive design [26–29,38]. Recent studies advocate for the integration of traditional passive techniques with modern performance evaluation tools to identify affordable and culturally appropriate retrofit strategies [7,8,19,30–32].

Most existing studies on passive energy efficiency strategies in buildings are based on urban or temperate climates and fail to account for the extreme environmental conditions and socio-cultural realities of high-altitude rural settlements like those in the Peruvian Andes [39–41]. This creates a contextual mismatch that limits the applicability of global best practices to Andean housing programs. Moreover, although optimization studies frequently demonstrate the benefits of passive design, they often propose solutions that are economically or technically unfeasible for low-income rural households [41,42]. As a result, there is a lack of research that evaluates affordable, locally viable retrofit strategies through simulation-based optimization methods tailored to the Andean context. Without such evidence, housing programs risk promoting interventions that are either ineffective or inaccessible to the communities they aim to serve [40].

This study focuses on optimizing the building envelope of the Sumaq Wasi modular house, a widely implemented public housing solution in high-altitude Andean regions, where Sumaq Wasi is a Quechua term referring to a good-quality or dignified dwelling. The research addresses three specific objectives. (1) To quantify the impact of feasible passive envelope modifications on indoor thermal discomfort under local climatic conditions. (2) To identify the envelope parameters that strongly influence thermal comfort using global sensitivity analysis. (3) To determine cost-effective combinations of passive retrofit strategies that minimize thermal discomfort and life cycle cost. These objectives are addressed using calibrated EnergyPlus simulations combined with sensitivity analysis and NSGA-II multi-objective optimization, The analysis focuses on passive envelope measures including insulation levels, thermal mass, airtightness-related parameters, and surface solar absorptance, within the technical and economic constraints of a standardized housing typology. To contextualize the economic relevance of passive interventions, the study includes a benchmark scenario using two 400W electric heaters. This benchmark represents a practical and readily available option that households may adopt to reduce cold discomfort. Since the base case has no space heating system, energy consumption is introduced rather than reduced. The primary objective is therefore not to minimize energy use, but to achieve acceptable indoor thermal conditions at the lowest possible life cycle cost. The findings support the identification of cost-effective envelope

 doi:10.20944/preprints202602.1796.v1



retrofit strategies that respond to local climatic conditions, resource limitations, and user behavior with the goal of improving indoor comfort for low-income households in the Peruvian Andes.

## 2. Materials and Methods

This study evaluates cost-effective passive strategies to improve thermal comfort in a government-built Sumaq Wasi modular house, representative of high-altitude rural housing in Peru. The methodology integrates field observations, empirical measurements, building energy simulation, sensitivity analysis, and multi-objective optimization. Field measurements were used to calibrate and validate the simulation model, while performance evaluation is conducted using simulation results. To evaluate the performance of the optimized solutions, three objective functions were defined, corresponding to the quantities minimized in the optimization: total discomfort, bedroom underheating, and life cycle cost. The evaluation compared the optimized passive designs against two benchmarks. The first benchmark was the base case, representing the existing Sumaq Wasi configuration without envelope modifications or space-heating systems. The second benchmark involved the use of 400W electric heaters in the bedrooms, included as a practical reference option for alleviating cold discomfort.

### *2.1. Study Context and Case Description*

The study was conducted in Langui, a district in the Cusco region of Peru located at an elevation of 3969 meters above sea level. Winter conditions are characterized by cold nights, intense solar radiation during the day, and significant daily temperature fluctuations (Figure 1). Residents face multiple socio-economic challenges, including inadequate housing quality, which, when combined with low night-time outdoor temperatures and strong radiative cooling under clear-sky conditions, result in harsh and often uncomfortable living environments.

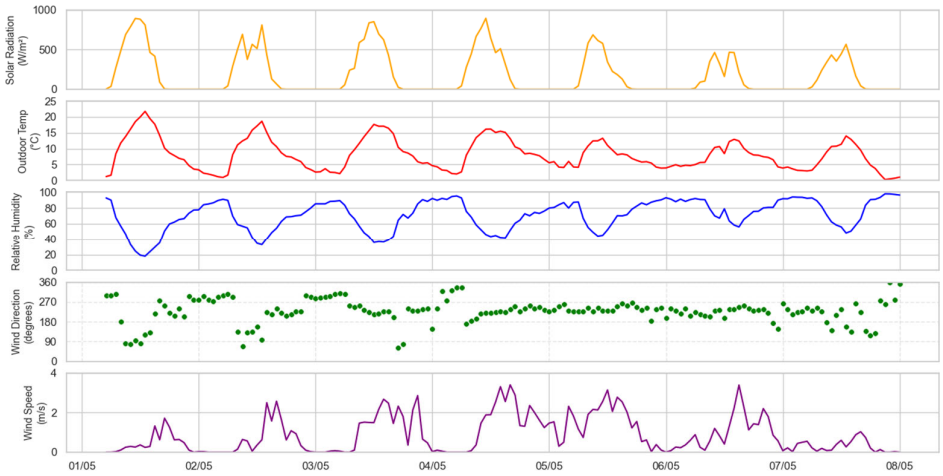


**Figure 1.** Hourly meteorological data use for EnergyPlus model calibration, recorded over a one-week measurement period in May 2023.

In response, the Peruvian government has implemented a rural housing program in the high Andes, introducing a modular house design known as Sumaq Wasi. These government-built dwellings in Langui have a typical floor area of 33 m² and feature adobe walls, an insulated metal roof, gypsum ceilings, and single-glazed windows (Figure 2 and Figure 3). The baseline construction systems and their thermal transmittance values are summarized in Table 1, which presents two Sumaq Wasi variants based on adobe and fire clay brick exterior walls. The table includes all major envelope components, including a skylight located in the main living space. Several envelope components exhibit relatively high U-values, indicating limited thermal resistance. Field

 doi:10.20944/preprints202602.1796.v1



observations and previous studies also indicate high infiltration rates and absence of any active heating systems [1]. These factors contribute to poor indoor thermal conditions. Consequently, residents often rely on adaptive behaviors, such as wearing multiple garments and using thick blankets, to cope with by cold indoor conditions [43].

**Figure 2.** View of a Sumaq Wasi house.

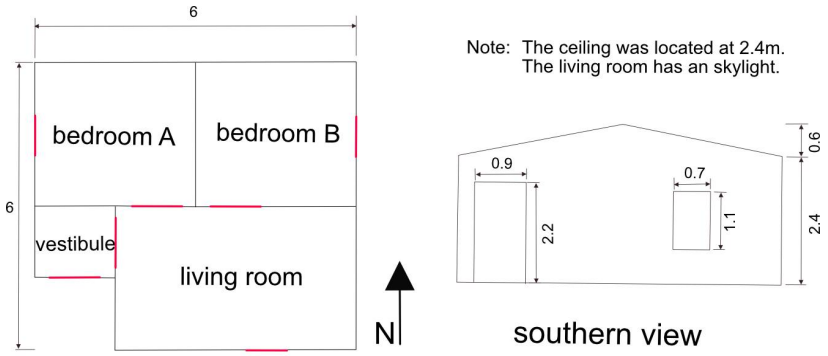


**Figure 3.** Geometry of the base case model.

**Table 1.** Constructions of the surfaces.

| | **Sumaq Wasi design with adobe as exterior wall main material** | | **Sumaq Wasi design with fired clay bricks as exterior wall main material** | |
|---|---|---|---|---|
| **Constructions** | *Material layers (from exterior to interior)* | *U value (W/m²•K)* | *Material layers (from exterior to interior)* | *U value (W/m²•K)* |
| Exterior walls | Adobe | 1.471 | Hollow clay brick<br>EPS<br>Hollow clay brick | 0.732 |
| Interior walls | Gypsum panel 0.0127<br>airgap<br>Gypsum panel 0.0127 | 2.22 | Hollow clay brick | 2.155 |
| Windows | Single glazing | 5.7 | Single glazing | 5.7 |
| Skylight | Transparent corrugated polycarbonate sheet | 5.59 | Transparent corrugated polycarbonate sheet | 5.59 |

 doi:10.20944/preprints202602.1796.v1



| | | | | |
|---|---|---|---|---|
| Ceiling | Vinyl-coated gypsum ceiling panel | 3.521 | Vinyl-coated gypsum ceiling panel | 3.521 |
| Roof | Painted Corrugated Galvanized Steel Sheet + Expanded polystyrene (EPS) | 0.583 | Painted Corrugated + Galvanized Steel Sheet + Expanded polystyrene (EPS) | 0.583 |
| Floor | Concrete floor slab + Gravel bedding layer | 2.775 | Concrete floor slab + Gravel bedding layer | 2.775 |
| Window´s shutter | Plywood + air gap + plywood | 2.805 | Plywood + air gap + plywood | 2.805 |
| Entrance door | Plywood + EPS + Plywood | 1.045 | Plywood + EPS + Plywood | 1.045 |
| Bedroom doors | Plywood + EPS + Plywood | 0.974 | Plywood + EPS + Plywood | 0.974 |

Although Table 1 presents two construction variants implemented with the Sumaq Wasi program, this study focuses exclusively on the adobe wall design. This choice reflects commonly recognized environmental considerations related to material availability, construction practices, and the use of locally sourced earth-based materials in rural Andean contexts [44,45]. Nevertheless, the fired clay brick wall configuration is retained as a benchmark case. It allows the performance of the optimized passive solutions to be evaluated against an alternative construction system that has also been implemented by the housing program.

*2.2. Simulation Model and Calibration*

A base case model was developed using EnergyPlus 24.2.0 to represent a typical Sumaq Wasi house. This dynamic building simulation software employs interconnected modules to calculate heating and cooling loads under specific environmental and operational conditions. Simulations are based on the heat balance method [46] that assumes uniform air temperature within a thermal zone's volume and homogeneous surface temperatures with one-dimensional heat conduction [47]. Additional assumptions include diffuse surface radiation emission and uniform irradiation. The model solves four core processes using energy conservation equations: heat balance on the exterior wall surface, one-dimensional heat conduction through walls, heat balance on the interior wall surface, and indoor air heat balance. Since the thermal zones analyzed in this study lacked active heating, cooling, and we assumed no air exchange with other zones, the indoor air heat balance simplifies accordingly [47]:

| energy stored in zone air [W] | = | sum of convective internal loads [W] | + | convective heat transfer from the zone surfaces [W] | + | heat transfer caused by air infiltration [W] |
|---|---|---|---|---|---|---|

$$C_a \frac{dT_i}{dt} = \sum_{j=1}^{N_{sl}} \dot{Q}_{l_j} + \sum_{k=1}^{N_{surfaces}} h_k A_k (T_{s_k} - T_i) + \dot{m}_{inf} c_p (T_o - T_i), \quad (1)$$

where:

$A_k$ = area of the zone surface $k$ [m²]

$c_p$ = specific heat of the air [J/(kg•K)]

 doi:10.20944/preprints202602.1796.v1



$C_a$ = air capacitance [J/K]
$h_k$ = convective heat transfer coefficient with surface $k$ [W/(m²•K)]
$\dot{m}_{inf}$ = air infiltration mass flow [kg/s]
$N_{sl}$ = number of convective internal loads [-]
$N_{surfaces}$ = number of surfaces in the thermal zone [-]
$\dot{Q}_{l_j}$ = heat from internal load $j$ [W]
$T_{s_k}$ = temperature of surface $k$ [K]
$T_i$ = indoor air temperature [K]
$T_o$ = outdoor air temperature [K]

The EnergyPlus model inputs were defined based on a combination of documented building specifications, field observations, and environmental data sources. Geometry, materials, and thermal properties were extracted from government reports, literature, and field studies [47,48] (Figure 2 and Table 1). Internal heat gains included one person per bedroom sleeping between 20:00 and 5:00 (70 W each); lighting loads of 100 W in the living room, and 50 W in each bedroom from 4:00-5:00, and 19:00-20:00. Window shutters were modeled as closed between 20:00 and 5:00. External meteorological inputs required by the simulation were provided through an EPW weather file. In this study, the Cusco EPW file was used. Model calibration was required to ensure that the simulated indoor temperatures realistically represent the thermal behavior of Sumaq Wasi dwellings under real operating conditions. Among the processes influencing the indoor air heat balance, air infiltration plays a dominant role in lightweight rural dwelling operating without active heating [9]. However, reliable references for infiltration characteristics of Sumaq Wasi houses are not available, which prevents direct specification of infiltration-related parameters. For this reason, calibration was carried out by comparing simulated and measured indoor air temperatures from 1-8 May 2023 (Figure 4). Three temperature sensors placed in one bedroom, while outdoor conditions were monitored with a nearby meteorological station (Table 2 and Figure 1)

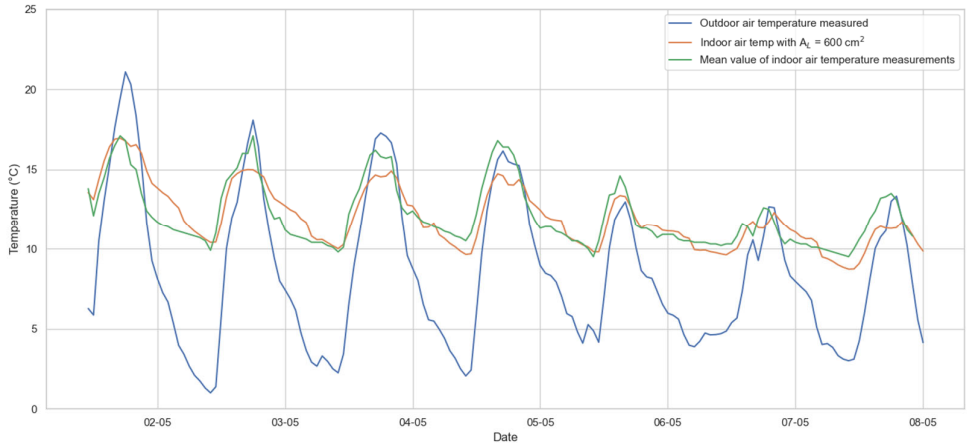


**Figure 4.** Result of calibration process

**Table 2.** Specifications of measurement instruments.

| Parameter measured | Name of instrument | Range | Accuracy |
|---|---|---|---|
| Indoor air temperature | Elitech RC-4HC | -40°C to +85°C | ±0.5°C |
| Solar radiation | ONSET smart sensor S-LIB-M003 | 0 to 1280 W/m2 | ±10W/m2 |

 doi:10.20944/preprints202602.1796.v1



| | | | |
|---|---|---|---|
| Outdoor air temperature | ONSET S-THC-M002 | -40°C to +75°C | ±0.20°C |
| outdoor air relative humidity | ONSET S-THC-M002 | 0 to 100% | ±2.5% |
| Wind direction | ONSET S-WCF-M003 | 0 to 355 degrees | ±7 degrees |
| Wind speed | ONSET S-WCF-M003 | 0 to 76 m/s | ±1.1 m/s |
| Data logger | HOBO RX3004 Remote Monitoring Station | - | - |

Air infiltration was modeled using the effective leakage area method implemented in EnergyPlus. In this formulation, infiltration is driven by buoyancy (stack) and wind effects, and it is expressed as:

$$V_{inf} = \frac{A_L}{1000}\sqrt{C_s(\Delta T) + C_w U^2}\ , \quad (2)$$

where:

$V_{inf}$ = air infiltration rate, $m^3/s$

$A_L$ = effective air leakage area, $cm^2$

$C_s$ = stack coefficient, $(L/s)^2/(cm^4 \bullet K)$, in our case equal to 0.0000145 according to [47]

$\Delta T$ = $T_i - T_o$, indoor-outdoor temperature difference, K

$C_W$ = wind coefficient, $(L/s)^2/[cm^4(m/s)^2]$, in our case equal to 0.000319 according to [47]

$U$ = local wind speed, m/s

The effective leakage area $A_L$ was treated as the calibration parameter and iteratively adjusted. The calibration identified $A_L$ = 600 $cm^2$ as the valued with the lowest error indicators (Figure 4): Normalized Mean Bias Error (NMBE) = 0.78 %; Root Mean Square Error (RMSE) = 1.03; Coefficient of Variation of RMSE (CV(RMSE)) = 8.51. This value was subsequently used for all base case simulations.

In addition to the calibrated base infiltration, adaptive window opening during overheating was represented by temporarily increasing the $A_L$ of the corresponding zone. When the operative temperature exceeded an upper comfort threshold, the effective leakage area was increased to simulate enhanced air exchange due to window opening. This approach directly modifies the infiltration term in Eq. (2), increasing the airflow driven by stack and wind effects. In the base case, the activation threshold was set to 25 °C and its influence was further examined in the sensitivity analysis.

### *2.3. Objective Functions*

Three objective functions were defined to evaluate the performance of the base case scenario. The first objective function was the Total Thermal Discomfort Index ($TDI_{total}$) defined as the annual sum of hourly deviations of operative temperature outside an acceptable comfort range in the bedrooms and living room. The comfort range was set between (14°C and 25°C) based on field measurements and occupant surveys conducted in Langui, reflecting locally adapted thermal comfort conditions [49]. Upper temperature limits were retained to ensure acceptable indoor conditions over the full diurnal cycle and to avoid optimization solutions that reduce cold discomfort at the expense of overheating. The $TDI_{total}$ was calculated as:

 doi:10.20944/preprints202602.1796.v1



$$TDI_{total} = \sum_{zone=1}^{3} TDI_{zone} \ where\ zone\ \in \{livingroom, bedroom_1, bedroom_2\} \quad (3)$$

where:

$$TDI_{zone} = \sum_{i=1}^{8760} \begin{matrix} 14 - T_{op}, & if\ T_{op} < 14°C \\ T_{op} - 25, & if\ T_{op} > 25°C \\ 0, & otherwise \end{matrix} \quad (4)$$

where $T_{op}$ denotes the operative temperature at hour $i$ of one room (°C), and 8760 is the number of hours during the simulated year.

The second objective function was the Thermal Discomfort Index due to Underheating in Bedrooms ($TDIU_{bedrooms}$), which specifically targets cold-related discomfort during sleeping hours. Unlike $TDI_{total}$, which accounts for both cold and warm deviations across all occupied spaces, this index considers only temperature deviations below 14°C and is evaluated exclusively in bedrooms. This objective reflects the most frequently reported thermal complaint in the community and prioritizes nighttime thermal conditions associated with health and well-being, and was defined as:

$$TDIU_{bedrooms} = \sum_{zone=1}^{2} TDIU_r \ where\ zone\ \in \{bedroom_1, bedroom_2\} \quad (5)$$

where

$$TDIU_{zone} = \sum_{i=1}^{8760} \begin{matrix} 14 - T_{op}, & if\ T_{op} < 14°C \\ 0, & otherwise \end{matrix} \quad (6)$$

The third objective function was the Life Cycle Cost ($LCC$) of the building over a 10-year evaluation period. The $LCC$ included both the initial investment cost for the envelope and heating systems, and the discounted operational cost of electricity used for heating. The operational costs were calculated monthly and aggregated annually, using a fixed discount rate $r$. $LCC$ was calculated following standard life-cycle cost assessment procedures [50,51]:

$$LCC = C_{inv} + \sum_{y=1}^{10} \frac{C_{op,y}}{(1+r)^y} \quad (7)$$

$C_{inv}$ : initial investment cost (USD)

$C_{op}$ : operating cost in year $y$ (USD/year)

$r$ : discount rate, set at 10% to reflect the high capital risk and local preference for minimizing upfront investments.

$C_{op}$ was assumed to include only electricity costs. In Langui, electricity tariffs follow a tiered block structure. For monthly consumption below 30 kWh, electricity is charged at 0.150 USD/kWh. For consumption between 31 and 140 kWh, the first 30 kWh are charged at a rate of 0.045 USD/kWh, while all additional consumption above 30 kWh is charged at 0.215 USD/kWh. For monthly consumption exceeding 140 kWh, a flat rate of 0.220 USD/kWh is applied to the entire consumption [52].

*2. ,4 Sensitivity Analysis*

A two-stage Global Sensitivity Analysis (GSA) was conducted. We adopted a two-stage approach commonly used in building performance studies [53–55]. First, we applied the Morris method (elementary effects) to screen and reduce the dimensionality of the input space by identifying the most impactful parameters [56,57]. Then, we performed a focused Sobol' analysis on this reduced

 doi:10.20944/preprints202602.1796.v1



set to quantify the contribution of each input variable and their interactions to the variance of the model outputs [56]. Both stages relied on Monte Carlo-based sampling strategies to systematically generate randomized combinations of input parameters, each of which was used to run an individual EnergyPlus simulation. This procedure enabled a comprehensive assessment of both main effects and higher-order interactions across the entire plausible range of each parameter.

The Morris method is a qualitative method that allows us to rank the variable according to their relative influence and allows us to screen the important variables. Here, the output of interest is a function $y(x)$ where $x$ is a vector of $k$ coordinates each representing an input variable, then $x = (x_1, x_2, x_3, \dots, x_k) \in \mathbb{R}^k$. Each coordinate is converted to a normalized value between 0 and 1 using $x_i^* = \frac{x_i - x_{min}}{x_{mx} - x_{min}}$. The space between 0 and 1 is divided into $p$ points that are decided by the user. After these definitions, the method starts but creating an initial point with random values of the variables, then it creates subsequent $k$ points changing one variable at a time a step $\Delta_i$, the selection of the modified variable is randomly chosen, and this group of $k+1$ points is called trajectory. To ensure equal probability for each value of each point, Morris suggested to make $p$ even and the step $\Delta_i = \frac{p}{2(p-1)}$. The method chose the direction of the step analyzing if $x_i$ is higher or lower than 0.5 to stay always inside the grid $(0,1)$ [55].

Then an indicator elementary effect $(EE)$ is defined to measure how much the output changes when only variable $x_i$ is changed:

$$EE_i = \frac{y(x + \Delta_i \cdot e_i) - y(x)}{\Delta_i} \tag{8}$$

Where, $e_i$ is a vector with 1 in the $i$-th position and 0 elsewhere. As for each trajectory the method only modified each $x_i$ once in all the steps, then the respective steps are selected to calculate $EE_i$. During the method $r$ amount of trajectories are created, then for each variable $i$ the standard mean $\mu_i$, the mean of absolute values $\mu_i^*$, and standard deviation $\sigma_i$ of the elementary effects are calculated [55]:

$$\mu_i = \frac{1}{r}\sum_{t=1}^{r} EE_{it} \tag{9}$$

$$\mu_i^* = \frac{1}{r}\sum_{t=1}^{r} |EE_{it}| \tag{10}$$

$$\sigma_i = \sqrt{\frac{1}{r-1}\sum_{t=1}^{r}(EE_{it} - \mu_i)^2} \tag{11}$$

Based on these indicators, the $i$ variables could be ranked according to their impact on the output $y(x)$. The size of $\mu$ gives information of the importance of the variable, but sometimes the mean values among trajectories could be positive or negative and cancel out, so $\mu^*$ was defined. The size of $\sigma$ gives information about the linearity or non-linearity of the effect, and its interaction with other variables. Thus, a variable with low $\mu^*$ and low $\sigma$ has a negligible effect; a variable with high $\mu^*$ and low $\sigma$ has important linear effect; and a variable with high $\mu^*$ and high $\sigma$ has important non-linear effects or interacting effects. In building simulation, non-linear and interacting effects are very common [55].

In this case, the Morris method was applied to two objective functions $y(x)$: $TDI_{total}$ and $TDIU_{bedrooms}$. The Morris method is used here as a screening tool to identify the most influential physical drivers of indoor thermal behavior. For this reason, the $LCC$ objective was not included in

 doi:10.20944/preprints202602.1796.v1



the sensitivity analysis, as its response to design modifications is directly computed from assigned unit costs, without complex physical interactions.

A total of $k$ = 20 input parameters were selected from the EnergyPlus model. These parameters represent envelope properties and key use-related inputs that can be modified and are relevant for indoor thermal performance (Table 3). The definition and range of each parameter are presented in the following subsection.

The Morris analysis was conducted using $p$ =4, uniformly spaced across their respective ranges. A total of $r$ = 50 trajectories was used to ensure robustness of the sensitivity indices[58,59], resulting in $r \times (k + 1)$ = 1050model evaluations.

**Table 3.** Envelope, geometry, and use-related parameters and their variation ranges used in the Morris sensitivity analysis.

| Desing variable | Range | Description |
|---|---|---|
| roof_u | [0.122-0.570] | U-value of the roof [W/K·m2] |
| exterior_wall_u | [0.291-1.471] | U-value of exterior walls [W/K·m2] |
| interior_wall_u | [0.28-2.22] | U-value of interior walls [W/K·m2] |
| floor_u | [0.149-3.33] | U-value of the floor [W/K·m2] |
| ceiling_u | [0.149-3.579] | U-value of the ceiling [W/K·m2] |
| window_u | [1.2-5.7] | U-value of windows [W/K·m2]. From base case up to four-layer single glass window with air gaps |
| interzone_door_u | [0.312-0.92] | U-value of interior doors [W/K·m2] |
| exterior_door_u | [0.398-2.538] | U-value of entrance door [W/K·m2] |
| srr | [0.033-0.131] | Skylight to roof ratio [-] |
| wwr | [0.036-0.145] | Window to wall ratio [-] |
| skylight_transparency | [0.2-0.8] | Transparency of the skylight [-] |
| internal_mass_ahc | [16051.2-4012.8] | Areal heat capacity of the zone's internal mass [J/m·K] |
| external_wall_extra_ahc | [49784.5-198738] | Areal heat capacity added to external walls [J/m·K] |
| internal_wall_extra_ahc | [49784.5-198738] | Areal heat capacity added to internal walls [J/m·K] |
| window_opening_upper_threshold | [2–9] | Degrees over 14°C when people open windows because of overheating [°C] |
| infiltration | [0.25-1] | Fraction of an effective leakage area of 2000 cm2 [-] |
| shutter_u | [0.312-0.92] | U-value of window shutters [W/K·m2] from an interior gap filled with 0.07m EPS to base case |
| people_activity_level | [25–100] | Heat produced by people inside zones [W] |
| rotation | [0–270] | Rotation angle from the north [°] |

 doi:10.20944/preprints202602.1796.v1



| | | |
|---|---|---|
| external_wall_solar_absorptance | [0.10- 0.95] | Solar absorptance of the exterior surface of exterior walls [-] |
| overhang_solar_transmittance | [0–75] | Solar transmittance of the roof's overhang |

Two variables, *infiltration* and *people activity level*, were included in the Morris screening stage to assess their relative influence, even though they are not controllable through design in the studied context. Infiltration is highly uncertain and largely dependent on construction quality, while activity level is governed by occupant behavior. Due to the lack of empirical evidence on how modifications to the building envelope could reduce infiltration, we did not explore design solutions targeting its mitigation. Furthermore, it is well established infiltration is one of the dominant parameters influencing thermal behavior in these types of buildings [9]. To prevent infiltration from overshadowing other parameters in the sensitivity analysis, its variation was restricted to a narrow range centered on the calibrated effective leakage area ($A_L = 600cm^2$), corresponding to 25-100% of this value (Table 3). While *people activity level* is also beyond the control of envelope design, it remains a critical factor as it represents the primary source of internal heat gains.

The second step of the GSA involved applying the Sobol method, a variance-based approach well suited for complex, nonlinear models such as those used in building energy simulation [56,60,61]. This method quantifies the extent to which output variance is attributable to individual input parameters or to their interactions. Due to its computational intensity, the Sobol method was applied only to a subset of the most influential variables identified during the Morris screening stage.

To determine which parameters to include in the Sobol analysis, we established thresholds based on the indicators $\mu^*$ and $\sigma$ from the Morris method. These thresholds were $\mu^* > 0.2 \cdot \max(\mu^*)$ and $\sigma > 0.5 \times \mu^*$. This approach aligns with screening criteria proposed in previous studies [57,62]. Additionally, the parameters *infiltration* and *people activity level* were excluded from the Sobol stage since they cannot be addressed through the envelope design strategies evaluated in the subsequent optimization. While both are influential, they fall outside the scope of design-controllable variables in this context.

The Sobol method decomposes the total variance of the model output $Y$, denote $V(Y)$, into additive terms that reflect the influence of individual input parameters and their interactions:

$$V(Y) = \sum_i V_i + \sum_{i<j} V_{i,j} + \sum_{i<j<k} V_{i,j,k} + \cdots \quad (12)$$

Where $V_i$ represents the first-order effect of parameter $X_i$, and $V_{i,j}$, $V_{i,j,k}$, … correspond to higher-order interaction effects. In this way, Sobol's method allows one to quantify the share of output variance attributable to each input variable, whether due to its direct influence or interactions.

For each parameter, two sensitivity indices were computed. The first-order Sobol index $S_i$ measures the effect of $X_i$ alone on the variance of $Y$:

$$S_i = \frac{V_{X_i}(E_{\sim i}[Y \mid X_i])}{V(Y)} \quad (13)$$

The total-order Sobol index $ST_i$ accounts for both the individual contribution of $X_i$ and all its interactions with other variables:

$$ST_i = 1 - \frac{V_{\sim X_i}(E_{X_i}[Y \mid X_{\sim i}])}{V(Y)} \quad (14)$$

In these expressions, $E[\cdot]$ denotes the expectation operator, i.e., the average of the model output over repeated sampling, and $V(\cdot)$ denotes the variance, which measures the dispersion around the mean. These operators are applied conditionally to isolate the effects of one or more parameters on the output variance.

 doi:10.20944/preprints202602.1796.v1



The Sobol indices were estimated using the Monte Carlo-based sampling scheme originally proposed by Sobol [61] and later refined by Homma and Saltelli [63]. This method constructs structured samples to efficiently approximate the sensitivity indices through model evaluations. Two $N \times k$ sampling matrices $A$ and $B$ are first generated, where $k$ is the number of input parameters and $N$ is the number of base samples. Then, hybrid matrices are built by swapping one column at a time between $A$ and $B$, yielding a total of $N \times (k + 2)$ simulations. In this study, $N$ = 512 was chosen to ensure robust estimation of the sensitivity indices, in line with established recommendations for building energy modeling [59].

Design variables for the GA optimization were selected using Sobol total-order indices. Parameters were ranked by their $ST_i$ and retained until their cumulative $ST_i$ exceeded 0.85, ensuring that the selected set captured the majority of output variance. Non-design factors (e.g., infiltration, occupant activity) were excluded from the optimization set.

### *2.5. Construction Alternatives*

We focused on selecting a range of possible construction alternatives to establish wide parameter bounds for the Morris and Sobol sensitivity analyses. The cost of each alternative was estimated only after identifying the most influential parameters. Because the Sumaq Wasi housing program operates under tight budget constraints, with each module costing approximately USD 8,100, our selection of construction modifications prioritized affordability, local material availability, and simplicity of implementation. For the sensitivity analysis, we sought to define broad variable ranges to ensure methodological robustness, without prematurely restricting options based on practical feasibility.

To model improvements in the thermal resistance of roofs, walls, floors, ceilings, doors, and shutters, we drew on the work of Juanicó and Gonzáles [64] and Juanicó [65]. These authors developed low-cost multilayer insulation panels combining expanded polystyrene (EPS), air gaps, and low-emissivity layers such as aluminum foil. Their findings showed that, for a 21°C temperature difference between indoor and outdoor environments, multilayer EPS-air panels outperformed solid EPS panels of equal thickness. Furthermore, lining the interior surface with aluminum foil significantly reduced radiative heat transfer, resulting in lower U-values at minimal additional cost.

Following this methodology, we calculated U-values for three multilayer configurations: solid EPS, EPS with air gaps, and EPS with both air gaps and aluminum foil. All insulation layers were assumed to be 0.01 m thick. For roof, floor, and ceiling assemblies, total insulation thicknesses up to 0.5 m were considered, producing U-values ranging from 3.5 to 0.068 W/m²·K. For exterior and interior walls, U-values ranged from 3.5 to 0.179 W/m²·K. A summary of the ranges produced by these construction alternatives is provided in Table 3.

Modifications to solar heat gains were also incorporated by adjusting the size of windows and skylights, represented by the variables *window-to-wall ratio (wwr)* and *skylight-to-roof ratio (ssr)*, respectively. Additionally, the orientation of the building with respect to true north was varied to evaluate the impact of solar exposure on thermal performance (Table 3). Local terrain shading from surrounding mountains was not explicitly modeled; solar access was therefore assumed to be unobstructed to isolate the influence of orientation and envelope-related design parameters

### *2.6. Optimization*

The optimization aimed to identify modifications to the Sumaq Wasi building that would minimize the three objective functions: $TDI_{total}$, $TDIU_{bedrooms}$, and $LCC$. Only the design parameters which cumulative $ST_i$ accounted for 0.85 of the total variance in the Sobol sensitivity analysis were considered in the optimization process, and the associated costs of their construction alternatives were estimated in advance. The range of values explored for each variable matched those used in the GSA (Table 3).

The optimization was performed using the Non-dominated Sorting Genetic Algorithm II (NSGA-II), implemented through multiple simulations using EnergyPlus and Python. GAs are population-based, stochastic optimization techniques widely used in building performance

 doi:10.20944/preprints202602.1796.v1



optimization due to their ability to explore large, nonlinear, and multi-dimensional design spaces [66–68].

In this framework, each candidate solution represents a specific combination of design variable values. For implementation within the GA, each solution is encoded as a chromosome, where each gene corresponds to one design variable in the simulation model. The performance of each candidate solution is evaluated by running the EnergyPlus model and computing the corresponding values of $TDI_{total}$, $TDIU_{bedrooms}$, and $LCC$.

The optimization proceeded over successive generations, through genetic operators such as selection, crossover, and mutation. NSGA-II extends conventional Gas by applying non-dominated sorting and elitism, enabling the identification of a Pareto-optimal front that represents trade-offs among the three objective functions [68,69].

### *2.7. Selection and Comparison of Optimized Solutions*

After constructing the Pareto front, a subset of optimized solutions was selected for detailed analysis based on their performance with respect to the three objective functions. We prioritized the solutions that exhibited the lowest values of $TDI_{total}$, $TDIU_{bedrooms}$, and $LCC$. They were labeled *optimized lowest* $TDI_{total}$, *optimized lowest* $TDIU_{bedrooms}$, and *optimized lowest* $LCC$, respectively, and a number was added to distinguish cases sharing the lowest value of any objective function.

To contextualize the performance of the optimized passive strategies, four benchmark scenarios were defined. The first was the unmodified base case, representing the standard Sumaq Wasi construction. The second benchmark consisted of the Sumaq Wasi variant with fired clay brick walls instead of adobe. The third scenario simulated the use of 400W electric heaters installed in the bedrooms and controlled by a thermostat with a heating setpoint of 14°C. In this scenario, heaters operate only when bedroom operative temperature falls below 14°C and are switched off otherwise. This solution considered both feasible and practical given local practices and affordability. The fourth benchmark represented an idealized reference case, in which electric heaters were used to fully prevent bedroom underheating by always maintaining operative temperatures at or above 14°C. This scenario was intended to estimate the minimum heating energy required to eliminate cold discomfort in bedrooms during sleeping hours. These benchmarks represent a spectrum of realistic and idealized adaptations that households may consider reducing nighttime cold discomfort.

All Pareto-optimal solutions identified through the optimization process were compared against these benchmarks using the three objective functions. This comparative evaluation provided valuable insights into the trade-offs and feasibility of passive design improvements versus conventional heating in high-altitude Andean housing.

## 3. Results

The Morris analysis identified the ceiling U-value as the most influential parameter for $TDI_{total}$ (Figure 5) and the exterior wall solar absorptance for $TDIU_{bedrooms}$ (Figure 6). The exterior wall U-value was also ranked among the most impactful variables for both objective functions. An increase in ceiling U-value reduced $TDI_{total}$ (negative $\mu$) but increased $TDIU_{bedrooms}$ (positive $\mu$), reveling a trade-off between daytime and nighttime performance: higher ceiling transmittance reduces overall annual discomfort while simultaneously worsening nighttime underheating in bedrooms.. In contrast, increasing roof U-value increased both $TDI_{total}$ and $TDIU_{bedrooms}$ ,highlighting the sensitivity of the dwelling's thermal behavior to roof heat transfer. Exterior wall solar absorptance showed a strong influence on $TDIU_{bedrooms}$, where higher absorptance reduced underheating discomfort, reflecting the importance of solar gains. The exterior wall U-value also exhibited consistent influence across both objective functions, confirming its role in governing heat exchange through the envelope.

 doi:10.20944/preprints202602.1796.v1



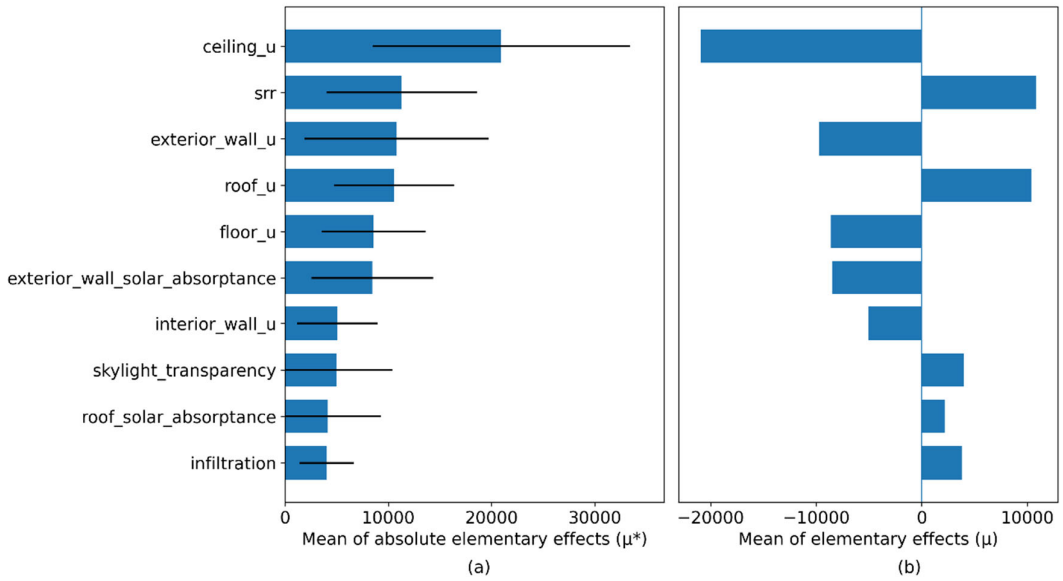


**Figure 5.** Morris sensitivity results for $TDI_{total}$: (a) $\mu^{\star}$ (importance) and $\mu$ (direction). Parameters are ordered by decreasing $\mu$ and only the ten highest-ranked variables are displayed.

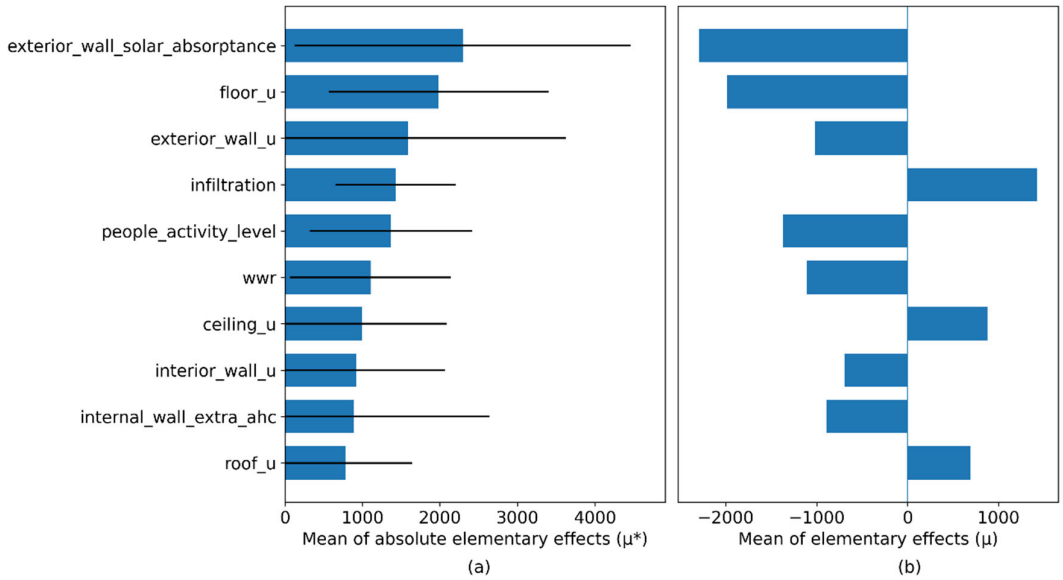


**Figure 6.** Morris sensitivity results for $TDIU_{bedrooms}$: (a) $\mu^{\star}$ (importance) and $\mu$ (direction). Parameters are ordered by decreasing $\mu$ and only the ten highest-ranked variables are displayed

Regarding solar gains, the skylight-to-roof ratio (SRR) ranked 2nd in importance for $TDI_{total}$ (Figure 5), where increasing SRR led to higher overall discomfort. In contrast, SRR ranked only 14th for $TDIU_{bedrooms}$, where increasing SRR reduced underheating. This behavior is consistent with increased solar irradiation through roof glazing. Additional solar gains help mitigate cold discomfort but intensify overheating during high-irradiation periods, leading to a net increase in annual total discomfort. Meanwhile, window-to-wall ratio (WWR) ranked 6th for $TDIU_{bedrooms}$ and 12th for $TDI_{total}$. Increasing WWR reduced both indicators. This suggests that vertical glazing provides beneficial solar gains during cold periods without substantially increasing overheating, indicating a different thermal role compared to skylights under the studied climate conditions.

In both objective functions, parameters such as the thermal mass of interior objects and exterior walls, as well as the transmittance of doors, shutters, and windows were consistently ranked as the

 doi:10.20944/preprints202602.1796.v1



least influential parameters. This does not imply that these parameters have no effect: rather, within the tested parameter ranges, their contribution to the variance of the discomfort indices was small relative to dominant factors. Across most variables, the magnitude of $\mu$ were similar to $\mu^*$, indicating limited sign changes in the elementary effects. This suggests that the direction of influence (positive or negative) remained consistent across the sampled trajectories, with minimal cancellation effects. In contrast, the relatively large values of $\sigma$ for several parameters indicate non-linear behavior and interaction effects within the explored parameter space.

For the Sobol analysis, thirteen parameters were retained based on the Morris screening results. Using the established thresholds ($\mu^* > 0.2 \cdot \max(\mu^*)$ and $\sigma > 0.5 \times \mu^*$), two screening plots were generated (Figure 7 & Figure 8). For $TDI_{total}$ , eight parameters exceed both thresholds, indicating a limited subset of influential variables with notable interaction effects. In contrast, fifteen parameters exceed the thresholds for $TDIU_{bedrooms}$, suggesting a broader sensitivity structure and stronger non-linear or interaction effects in the underheating response. All eight parameters identified for $TDI_{total}$ were also among those for $TDIU_{bedrooms}$. From this set, infiltration, and people activity level were excluded from the Sobol analysis due to their classification as non-design parameters, resulting in a final subset of thirteen design variables,

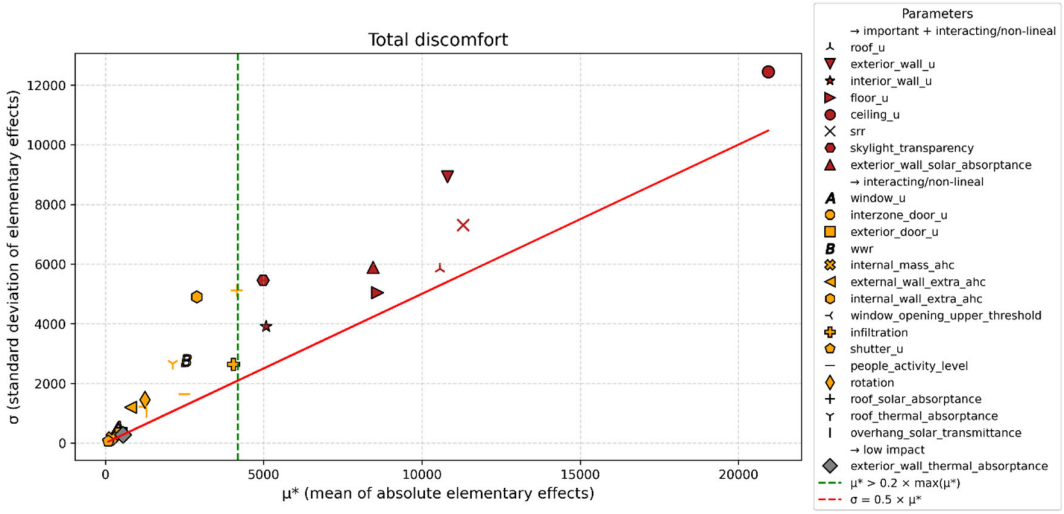


**Figure 7.** Morris screening results for $TDI_{total}$

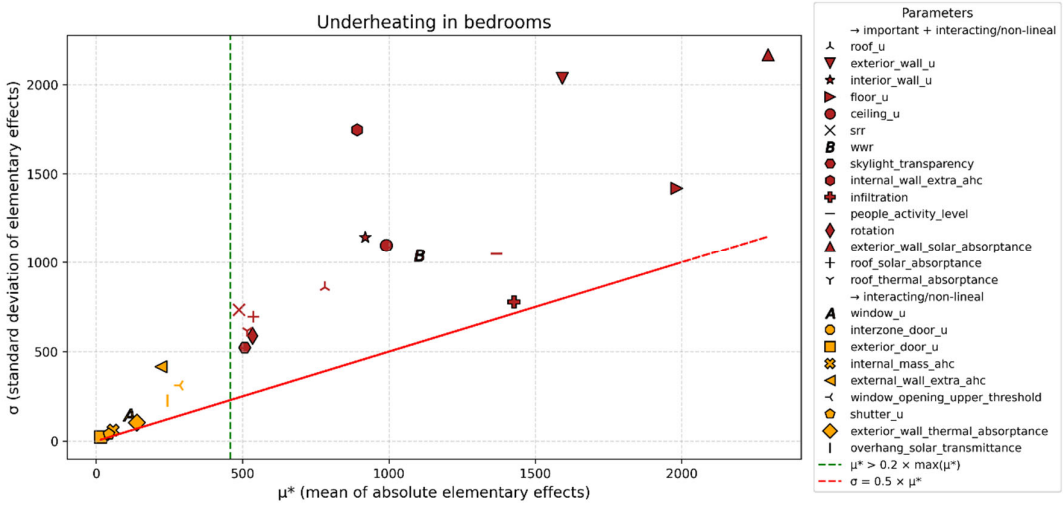


**Figure 8.** Morris screening results for $TDIU_{bedrooms}$

 doi:10.20944/preprints202602.1796.v1



The Sobol method revealed that for $TDI_{total}$, the most influential parameters were the thermal transmittance of ceiling and roof, the SRR, the thermal transmittance of exterior wall, and the exterior wall solar absorptance (Figure 9). For $TDIU_{bedrooms}$ the key contributors were exterior wall solar absorptance, floor thermal transmittance, the thermal mass of the interior walls, and the thermal transmittance of both exterior and interior walls (Figure 10). Collectively, these parameters accounted for more than 85% of the output variance. Several other parameters exhibited first-order ($S_i$) and total-order ($ST_i$) Sobol indices with confidence intervals extending to or near zero, suggesting their individual contributions were negligible or indistinguishable from noise given the dominance of the primary factors. In the case of $TDIU_{bedrooms}$, $S_i$ indices were substantially higher than the corresponding $ST_i$ indices for parameters such as floor, exterior walls, interior walls, and ceiling thermal transmittance, as well as for the thermal mass of interior walls (Figure 9 & Figure 10). This suggests stronger interaction effects among input parameters for $TDIU_{bedrooms}$ compared to $TDI_{total}$, where the $S_i$ and $ST_i$ values were generally more aligned across all parameters.

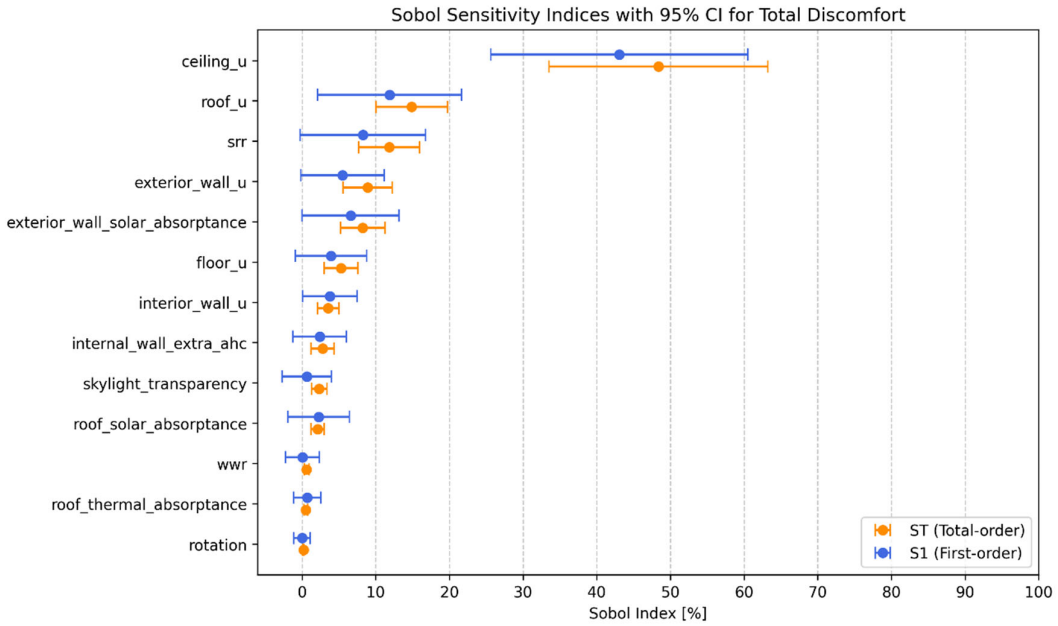


**Figure 9.** Sobol sensitivity indices with confidence interval for $TDI_{total}$.

 doi:10.20944/preprints202602.1796.v1



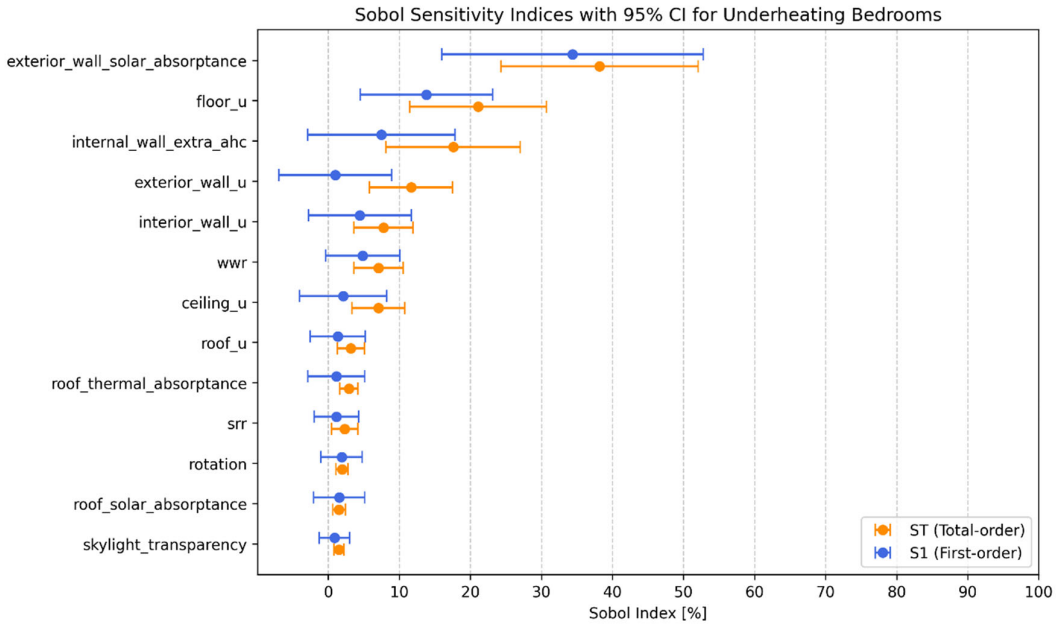


**Figure 10.** Sobol sensitivity indices with confidence interval for $TDIU_{bedroom}$

Only the parameters that collectively accounted for more than 85% of the variance of each objective function in the Sobol analysis were retained for the optimization (Table 4). These included the thermal transmittance of, ceiling, roof, exterior and interior walls, and floor, together with the SRR, exterior wall solar absorptance, and the thermal mass of interior walls. For each parameter, discrete design alternatives were defined based on realistic construction modifications within the ranges identified in the sensitivity analysis. Investment costs were estimated using local supplier price data collected in Cusco (2023) and represent material-only costs for envelope modifications relative to the base case.

The NSGA-II algorithm was configured with a population size of 50and 100 generations, producing a Pareto front of 50 optimal solutions. From this set, six representative configurations were selected (Table 5): Solutions 01 to 04 that are the four pareto solutions with the lowest $LCC$, solution 05 that had the lowest $TDIU_{bedrooms}$, and solution 06 that had the lowest $TDI_{total}$,. The four lowest $LCC$ pareto solutions (solutions 01 to 04) maintained an $LCC$ of 8,100 USD with a $TDI_{total}$ ranging from 8953°C·h up to 12,067°C·h and $TDIU_{bedrooms}$ ranging from 618°C·h up to 998°C·h. Solution 05 achieved a $TDIU_{bedrooms}$ equal to 164°C·h with an $LCC$ of 10059 USD. Solution 06 achieved a $TDI_{total}$ equal to 3437°C·h at a $LCC$ of 10457USD.. These solutions represent distinct trade-offs along the Pareto front

**Table 4.** Design parameter alternatives and associated material costs considered in the NSGA-II optimization

| Ceiling | | Exterior wall | | Floor | | Interior wall | | Roof | | Exterior wall solar absorptance | | Extra thermal mass interior walls | | SRR | |
|---|---|---|---|---|---|---|---|---|---|---|---|---|---|---|---|
| U-value (W/m2·K) | Cost (USD) | U-value (W/m2·K) | Cost (USD) | U-value (W/m2·K) | Cost (USD) | U-value (W/m2·K) | Cost (USD) | U-value (W/m2·K) | Cost (USD) | - | Cost (USD) | [J/m·K] | Cost (USD) | [-] | Cost (USD) |
| 3.521 | 0 | 1.471 | 0 | 2.775 | 0 | 2.22 | 0 | 0.583 | 0 | 0.9 | 0 | 0 | 0 | 13.1 | 0 |
| 1.755 | 398 | 0.549 | 1060 | 1.548 | 398 | 0.628 | 866 | 0.5 | 406 | 0.8 | 0 | 198738 | 700 | 9.8 | 0 |
| 1.254 | 567 | 0.474 | 1171 | 1.144 | 567 | 0.532 | 957 | 0.449 | 578 | 0.6 | 0 | | | 6.6 | 0 |
| 0.701 | 580 | 0.418 | 1282 | 0.665 | 580 | 0.462 | 1048 | 0.35 | 592 | 0.4 | 0 | | | 3.3 | 0 |
| 0.584 | 641 | 0.373 | 1393 | 0.559 | 641 | 0.408 | 1139 | 0.318 | 653 | 0.3 | 0 | | | | |
| 0.394 | 749 | 0.338 | 1504 | 0.383 | 749 | 0.366 | 1229 | 0.252 | 764 | 0.2 | 0 | | | | |
| 0.320 | 810 | 0.337 | 1590 | 0.312 | 810 | 0.365 | 1300 | 0.219 | 826 | | | | | | |
| 0.231 | 931 | 0.308 | 1615 | 0.227 | 931 | 0.331 | 1320 | 0.173 | 949 | | | | | | |
| 0.219 | 1046 | 0.295 | 1701 | 0.215 | 1046 | 0.316 | 1391 | 0.166 | 1066 | | | | | | |
| 0.166 | 1113 | 0.283 | 1726 | 0.164 | 1113 | 0.302 | 1411 | 0.134 | 1135 | | | | | | |
| 0.149 | 1235 | | | 0.148 | 1235 | 0.28 | 1481 | 0.123 | 1259 | | | | | | |

**Table 5.** Representative Pareto-optimal solutions selected from the NSGA-II optimization, including configurations minimizing $LCC$, $TDI_{total}$, and $TDIU_{bedrooms}$.

| Indicator | Units | Lowest $LCC$ | | | | Lowest $TDIU_{bedrooms}$ | Lowest $TDI_{total}$ | Base case | Sumaq Wasi fired clay bricks | Sumaq Wasi - Ideal electric heaters | Sumaq Wasi - 2x400W electric heaters |
|---|---|---|---|---|---|---|---|---|---|---|---|
| | | 01 | 02 | 03 | 04 | 05 | 06 | | | | |
| $LCC$ | USD | 8100 | 8100 | 8100 | 8100 | 10059 | 10457 | 8100 | 8100 | 8370 | 8506 |
| $TDI_{total}$ | [°C·h] | 8953 | 9224 | 10440 | 12067 | 4476 | 3437 | 15756 | 37016 | 33445 | 38792 |
| $TDIU_{bedrooms}$ | [°C·h] | 998 | 814 | 699 | 618 | 164 | 270 | 2077 | 1872 | 47 | 684 |
| Parameters | | | | | | | | | | | |
| Roof U-value | [W/K·m2] | 0.583 | 0.583 | 0.583 | 0.583 | 0.123 | 0.123 | 0.583 | 0.583 | 0.583 | 0.583 |

| | | | | | | | | | | | |
|---|---|---|---|---|---|---|---|---|---|---|---|
| Exterior wall U-value | [W/K·m2] | 1.471 | 1.471 | 1.471 | 1.471 | 1.471 | 1.471 | 1.471 | 0.732 | 1.471 | 1.471 |
| Ceiling U-value | [W/K·m2] | 3.521 | 3.521 | 3.521 | 3.521 | 3.521 | 3.521 | 3.521 | 3.521 | 3.521 | 3.521 |
| Floor U-value | [W/K·m2] | 2.775 | 2.775 | 2.775 | 2.775 | 2.775 | 1.548 | 2.775 | 2.775 | 2.775 | 2.775 |
| SRR | [-] | 3.3 | 6.6 | 9.8 | 13.1 | 13.1 | 6.6 | 9.8 | 9.8 | 9.8 | 9.8 |
| Exterior wall solar absorptance | [-] | 0.9 | 0.9 | 0.9 | 0.9 | 0.9 | 0.9 | 0.5 | 0.5 | 0.5 | 0.5 |
| Interior wall U-value | [W/K·m2] | 2.22 | 2.22 | 2.22 | 2.22 | 2.22 | 2.22 | 2.22 | 2.155 | 2.22 | 2.22 |
| Interior wall additional heat capacity | [J/m·K] | 0 | 0 | 0 | 0 | 198738 | 198738 | 0 | 0 | 0 | 0 |
| Heating systems | [-] | No | No | No | No | No | No | No | No | 2xIdeal electric heaters | 2x400W electric heaters |

 doi:10.20944/preprints202602.1796.v1



Across all selected configurations, exterior wall solar absorptance increased from 0.5 to 0.9 relative to the base case, highlighting the importance of solar gains. In Solution 06 (lowest $TDI_{total}$), the roof and floor U-values were reduced and SRR decreased, while interior walls thermal mass increased, which in practice meant to replace the air gap from the base case with adobe walls. In Solution 05 (lowest $TDIU_{bedrooms}$)roof U-value decreased and both SRR and interior walls thermal mass increased. The four lowest $LCC$ Pareto solutions primarily differed in their SRR values: higher SRR increased $TDI_{total}$ but reduced $TDIU_{bedrooms}$. None of the selected modifications modified the U-values of the exterior walls, ceiling, or interior walls relative to the base case.

To benchmark the cost of avoiding bedroom underheating, we computed two heating cases. First, we estimated the ideal heating requirement, defined as the monthly heating energy and peak power that would be necessary to maintain bedroom operative temperatures at or above 14°C at all times (unlimited heating capacity; Figure 11). Second, we simulated a capacity-limited case with two fixed 400 W electric heaters (one per bedroom) controlled with a 14 °C on/off thermostat (Figure 12). Heating demand occurred throughout most months of the year due to persistent nighttime operative temperatures below 14°C, typical of these high-altitude locations. In the ideal case, June had the highest heating demand (89 kWh) and a peak power requirement of 0.89 kW, resulting in an electricity cost of 14 USD under the local tariff. In the 2x400 W case, June electricity use increased to 114 kWh (19 USD). Despite the added electricity use, the 2x400W case does not eliminate underheating during cold hours, which results in a higher annual $TDIU_{bedrooms}$ (684 °C•h) than the ideal requirement benchmark (47°C•h).

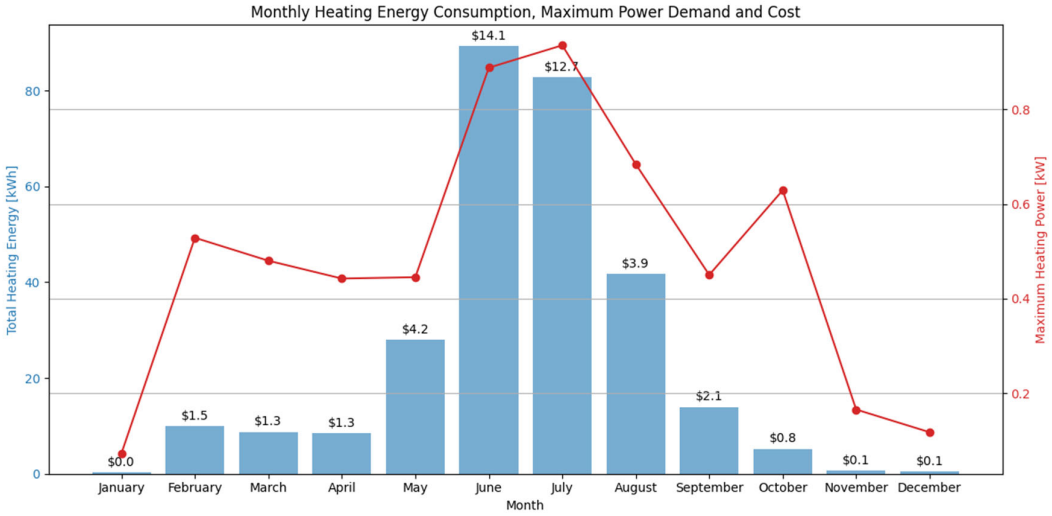


**Figure 11.** Ideal heating requirement for the two bedrooms: monthly heating energy and peak power needed to maintain operative temperature over 14°C

 doi:10.20944/preprints202602.1796.v1



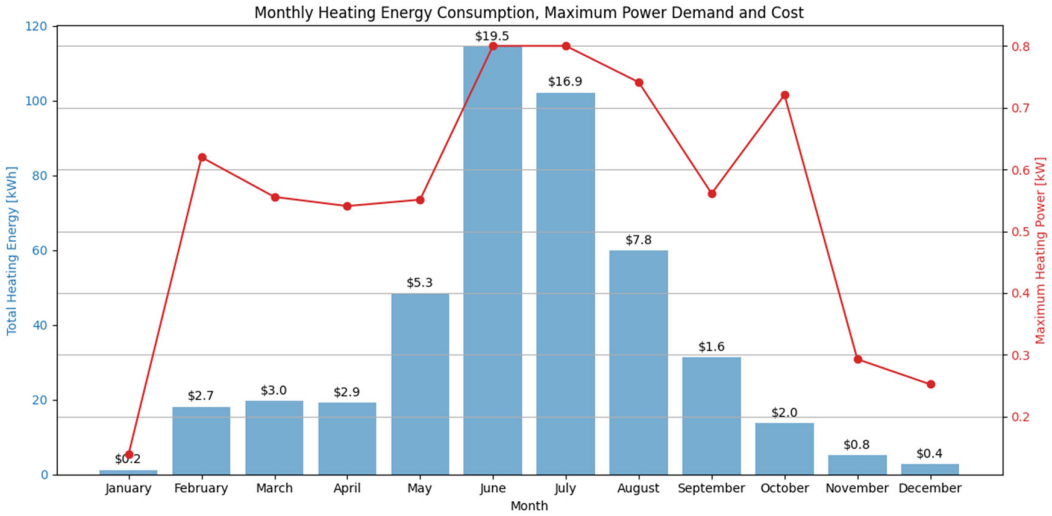


**Figure 12.** Capacity-limited electric heating case (2×400 W, one per bedroom): monthly electricity consumption and peak power with on/off control at 14°C

Figure 13 compares the six solutions selected from the Pareto-front (Table 5) against four benchmarks: the unmodified base case, the fired-clay variant, the 2x400W heater case, and the ideal heating requirement case. The Pareto solutions clustered in the lower $TDI_{total}$ relative to the base case, indicating that envelope modifications reduce annual total discomfort without introducing operational electricity use. occupy the low. The ideal heating requirement case yielded the lowest $TDIU_{bedrooms}$ by definition, but it was not considered a feasible option because it assumes unrestricted heating capacity with perfect control... Among the feasible alternatives, the solution minimizing $TDIU_{bedrooms}$ (Solution 05) achieved the lowest bedroom underheating within the Pareto set at moderate $LCC$. If cost is prioritized, Solution 04 provides the lowest $LCC$ among the six Pareto solutions while reducing bedroom underheating relative to the base case through higher SRR and higher exterior wall solar absorptance. . Notably, Solution 04 also resulted in lower $TDIU_{bedrooms}$ than the 2x400 W heater case while avoiding additional electricity use.

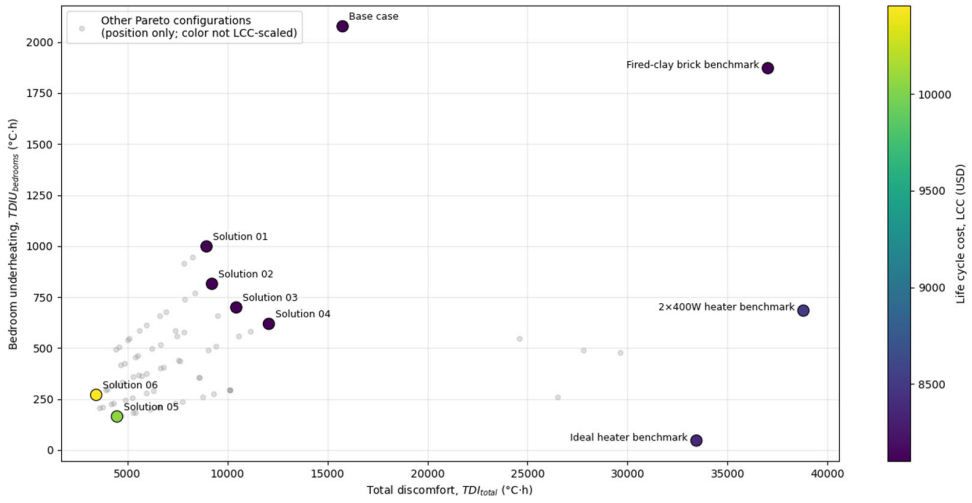


**Figure 13.** Trade-off between $TDI_{total}$, $TDIU_{bedrooms}$, and $LCC$ for the six solutions selected from the Pareto-front (Table 5) and benchmark cases. Faint gray points correspond to additional Pareto-optimal configurations and are shown only in objective space; their color does not encode $LCC$.

 doi:10.20944/preprints202602.1796.v1



## 4. Discussion

This study evaluated envelope modifications to a standardized public housing dwelling to improve indoor thermal comfort in high-altitude rural Peru. Solution 06 minimized total discomfort ($TDI_{total}$ =3437 °C·h; $LCC$ =10,457 USD), while Solution 05 minimized bedroom underheating ($TDIU_{bedrooms}$ = 164 °C·h;$LCC$ = 10,059 USD). These correspond to reductions to 22% and 8% of the base case values for $TDI_{total}$ and $TDIU_{bedrooms}$, respectively, with associated $LCC$ increases of 2,357 USD and 1,959 USD. A low-cost envelope modification consisting of increasing exterior wall solar absorptance to 0.9, and the SRR to 13.1 reduced $TDI_{total}$ to 12,067 °C·h and a $TDIU_{bedrooms}$ to 618 °C·h (77% and 30% of the base case, respectively) while maintaining the same $LCC$, assuming that wall color selection and semi-transparent roofing did not alter investment costs. Notably, this passive configuration achieved lower bedroom underheating than the 2x 400W electric heater case which yielded $DIU_{bedrooms}$ = 684 °C·h, and $LCC$ = 8506 USD.

A key limitation of this study relates to the modeling of infiltration. Infiltration strongly influences indoor temperatures in high-altitude dwellings due to large diurnal temperature differences. Although the GSA indicated moderate sensitivity within the selected parameter range, this was primarily a consequence of constraining the infiltration range. Large variations in infiltration rates would substantially alter thermal performance outcomes. Infiltration has opposing seasonal effects: it increases heat losses during cold periods but may reduce overheating during warm hours. Therefore, its net influence on annual discomfort reflects a trade-off between underheating and overheating. The selected Effective Leakage Area ($A_L$) value was determined through calibration against field measurements. While this approach improved model reliability, it does not capture short-term variability such as intermittent door openings. Consequently, the results should be interpreted assuming similar infiltration conditions. Given that public housing programs replicate the same construction typology and usage patterns, this assumption is considered reasonable. Expanding monitoring campaigns would further strengthen future analyses.

Despite these limitations, this study advances the understanding of building thermal behavior in rural high-altitude regions of the Peruvian Andes. Indoor air temperatures in such buildings are highly influenced by outdoor climatic conditions characterized by large diurnal temperature variations. However, energy simulation studies addressing tropical mountainous climates at high elevations remain limited. By combining sensitivity analysis with multi-objective optimization, this study provides quantitative evidence to support envelope design and retrofit decisions in public housing programs adapted to regional conditions. The analysis focused solely on low-cost, technically simple interventions that are feasible within the local social and economic context. This contrasts with much of the building simulation literature, which frequently evaluates advanced solutions that may not be applicable to low-income rural communities. Prioritizing practical, low-tech modifications enables more informed decision-making under financial constraints. The systematic sensitivity analysis further supports this objective by identifying parameters with the greatest influence on thermal performance, thereby assisting in the prioritization of interventions. An additional contribution of this study is the comparison between passive envelope upgrades and electric heating over a ten-year life cycle period. Although electric heating is not proposed as a viable long-term solution for low-income households, it serves as a benchmark to evaluate whether passive improvements are economically justified. This comparison provides a transparent framework for assessing the cost-effectiveness of envelope strategies and may inform policy decisions regarding the allocation of public resources to reduce indoor thermal discomfort in vulnerable populations.

When comparing these results with the existing literature, it is important to recognize that parameter significance is inherently dependent on the climatic context, building typology, and modelling assumptions. Therefore, the influence of individual parameters identified here should be interpreted within the specific conditions evaluated in this study. Research on rural buildings in the Andean region has primarily focused on mitigating low nighttime indoor temperatures, particularly during frost periods that pose health risks to children and the elderly [9,10,12,26,27]. Our findings extend this perspective by evaluating thermal comfort throughout the entire day. Although rural

 doi:10.20944/preprints202602.1796.v1



lifestyles often involve outdoor daytime activities, occupants such as elderly or ill individuals may remain indoors for extended periods, making whole-day thermal performance relevant.

Previous studies in the Andes have examined passive strategies including skylights [12,24], attached greenhouses [6,8,12,22,24], increased thermal mass from earth materials [6,12,22,24,26,27] , exposing natural earth floors [6,9,22], improved roof insulation [6,9,12,22,27], increased airtightness [6,7,9,12,22,24], and the use of double-glazed windows with shutters [9,12]. Consistent with this literature, the present study identified skylight area, interior wall thermal mass, floor transmittance, and roof transmittance as influential design parameters within the evaluated configuration space.

Notably, the Pareto-optimal solutions obtained through genetic algorithm optimization did not favor reducing exterior wall transmittance via added insulation. This result highlights the advantage of heat storage in wall surfaces through thermal mass rather than further increasing insulation, under the climatic conditions studied. In high-altitude tropical climates characterized by strong diurnal temperature variation and high solar radiation, storing daytime solar gains and releasing them during nighttime hours may be more beneficial than simply minimizing conductive heat losses. Additional insulation may reduce useful daytime solar heat gains without proportionally improving nighttime thermal conditions.

For the floor, the Pareto set revealed a trade-off between transmittance and the two discomfort metrics. The configuration minimizing $TDI_{total}$ exhibited the lowest floor transmittance, whereas the configuration minimizing $TDIU_{bedrooms}$ exhibited the highest transmittance (i.e., exposed earth floors). This pattern aligns with reports that exposed earth floors can dampen daytime temperature peaks due to thermal mass [6,22], and with studies suggesting that omitting floor insulation may improve night-time thermal conditions [22], although other studies report contrasting results [7,24]. The results also highlight the importance of thermal mass in interior walls, a parameter rarely examined in the literature, likely because traditional Andean rural dwellings are typically single-room structures [9]. As suggested in [9] and confirmed here, not all intuitive modifications, such as simply increasing insulation, lead to improved thermal performance; their effectiveness depends on the overall building configuration and climate context.

One parameter that has received comparatively little attention is the solar absorptance of exterior walls. In our study, all selected Pareto configurations adopted the maximum tested solar absorptance value (0.9), which reduced $TDI_{total}$ and $TDIU_{bedrooms}$ without additional investment, assuming wall color change is cost-neutral. This finding is consistent with the recognized role of wall heat storage and supports the relevance of wall solar absorptance in high-altitude Andean dwellings. Although darker wall colors would offer the greatest benefit, cultural acceptability should be considered. Earth-toned dark colors could offer a middle ground and merit further investigation. Finally, although roof solar reflectance has been widely examined (e.g. [30]), in our analysis, roof solar absorptance was not among the most impactful parameters.

An important trade-off arises when modifying the skylight-to-roof ratio (SRR). Although skylights are often recommended for these houses, our results indicate that increasing SRR tended to reduce $TDIU_{bedrooms}$ while increasing. This suggests that greater solar gains may alleviate cold nighttime conditions but can increase daytime discomfort under certain conditions. While severe overheating is unlikely in this climate, elevated daytime operative temperatures may reduce comfort during occupied hours. A comprehensive design strategy should therefore consider comfort across the full 24-hour cycle. Future work should quantify this trade-off and evaluate measures (e.g., selective glazing, internal blinds, or adjustable shutters) to capture solar gains while moderating daytime temperature peaks.

To maintain indoor temperatures above 14 °C over a full year, the Sumaq Wasi dwelling required 290 kWh of heating (≈ 0.9 kWh/day; 8.8 kWh·m$^{-2}$·year$^{-1}$). Operating two 400 W electric heaters resulted in an annual demand of 436 kWh (≈ 1.5 kWh/day; 13.2 kWh·m$^{-2}$·year$^{-1}$). For comparable bioclimatic buildings, Molina et al. [8] estimated daily energy needs of 4.2 kWh and 7.6 kWh for a minimum indoor temperature of 12.4 °C, and Iruri-Ramos et al. [22] reported 55.38 kWh·m$^{-2}$·year$^{-1}$. In both cases, the Sumaq Wasi design used less energy than these passive

 doi:10.20944/preprints202602.1796.v1



alternatives, underscoring its effectiveness. Moreover, the two-heater scenario also remained below those reported figures, making it advantageous from an energy perspective. While we recognize that electricity bills may pose a burden for low-income households, these findings suggest under the studied conditions, electric heating may represent a lower cost intervention than some passive alternatives. This comparison provides a basis for future policy discussions regarding thermal comfort strategies in vulnerable populations.

Future research should address the uncertainties associated with modeling infiltration and evaluating the effectiveness of measures intended to reduce it. As shown in this study and others in the literature, indoor comfort in this type of building is highly sensitive to infiltration rates. In our case, the model was calibrated using field measurements; however, to enhance the robustness of the model and its outputs, additional data should be collected, and more Sumaq Wasi dwellings should be calibrated to assess this parameter more thoroughly. Further studies should aim to quantify the airtightness of these buildings using conventional methods such as blower door tests. Although such field studies require additional resources, they would provide valuable insights into the potential impact of simple measures, such as improving door and window frame sealing, on reducing infiltration. While this study did not include infiltration-reduction measures due to the lack of data on the effectiveness of such interventions, it is widely accepted that decreasing infiltration can significantly enhance indoor comfort.

The findings of this study provide an evidence-based foundation for designing low-cost, thermally comfortable housing in high-altitude rural regions. By prioritizing simple, context-appropriate passive measures and evaluating them through robust simulation and optimization methods, we offer realistic alternatives for improving well-being in vulnerable communities. If implemented at scale, these strategies could reduce health risks, alleviate energy poverty, and enhance the effectiveness of public housing programs in high-altitude regions.

## 5. Conclusions

This study aimed to optimize the envelope design of a standardized dwelling from the Sumaq Wasi housing program using passive strategies and evaluated performance in terms of thermal comfort and life cycle cost. The solution minimizing total discomfort reduced $TDI_{total}$ to 22% of the base case value, while the solution minimizing bedroom underheating $TDIU_{bedrooms}$ to 8% of the base case. These improvements required additional investments of USD 2,347 and 1,959 USD, respectively, relative to the base case cost (USD 8,100).

A cost-neutral modification combining exterior wall solar absorptance (0.9) and higher skylight-to-roof ratio (SRR = 13.1) reduced total discomfort and bedroom underheating to 77% and 30% of the base-case values, respectively. This passive configuration outperformed the installation of two 400W electric heaters in terms of bedroom underheating while avoiding additional operational electricity costs.

Methodologically, this study demonstrates the value of combining global sensitivity analysis (Morris and Sobol) with multi-objective genetic algorithm optimization to identify context-appropriate passive design strategies under conditions of financial constraints and climatic severity. The comparison with electric heating provides a transparent benchmark for evaluating the economic efficiency of passive envelope upgrades in high-altitude rural housing.

These findings offer evidence to support more targeted investments in public housing programs serving vulnerable populations in the rural Andes. By prioritizing interventions with the highest impact per unit cost, housing initiatives can improve indoor thermal comfort while using limited resources more effectively.

**Author Contributions:** Conceptualization, E.M.S. and T.G.; methodology, E.M.S. and T.G.; software, E.M.S. and T.G.; validation, E.M.S.; formal analysis, E.M.S..; investigation, E.M.S. and T.G.; resources, E.M.S..; data curation, E.M.S and T.G..; writing—original draft preparation, E.M.S.; writing—review and editing, E.M.S. and B.P..;

 doi:10.20944/preprints202602.1796.v1



visualization, E.M.S.; supervision, E.M.S. and B.P.; project administration, E.M.S. and T.G.; funding acquisition, E.M.S. and T.G.. All authors have read and agreed to the published version of the manuscript.

**Funding:** Enrique Mejia-Solis acknowledges support from the FONDECYT/CONCYTEC "Generación Científica – Becas Internacionales" Ph.D. Scholarship Program (Award No. 303-2014).

**Data Availability Statement:** The data presented in this study are available on request from the corresponding author.

**Acknowledgments:** The authors would like to thank Jaime Arias, Associate Professor at the Department of Energy Technology, KTH Royal Institute of Technology, for his valuable guidance and constructive comments throughout the development of this study. We also sincerely acknowledge Francisco Oblitas for his support with the logistical coordination of the field measurements.

During the preparation of this manuscript, the authors used ChatGPT (version 5.2, OpenAI) for language editing and improvement of clarity. The authors have reviewed and edited the output and take full responsibility for the content of this publication.

**Conflicts of Interest:** The authors declare no conflict of interest.

## Abbreviations

The following abbreviations are used in this manuscript:

| | |
|---|---|
| $TDI_{total}$ | Total thermal discomfort |
| $TDIU_{bedrooms}$ | |
| $LCC$ | Life cycle costs |
| GAs | Genetic algorithms |
| NSGA-II | Non-dominated sorting genetic algorithm II |
| NMBE | Normalized mean bias error |
| RMSE | Root mean square error |
| USD | United States dollar |
| GSA | Global sensitivity analysis |
| $EE$ | Elementary effects |
| EPS | Expanded Polystyrene |
| WWR | Window to wall ratio |
| SSR | Skylight to roof ratio |

## References

1. E. Palomino-Olivera, M. Ancco-Peralta, V. Salas Velásquez, E. Mejia-Solis, and E. Gudiel Rodriguez, "Regulatory Gap Versus Performance Reality: Thermal Assessment of a Social Housing Module in the Peruvian Andes," *Buildings*, vol. 15, no. 24, p. 4401, Dec. 2025, doi: 10.3390/buildings15244401.
2. Á. Canales Gutiérrez, G. Belizario Quispe, A. P. Calatayud Mendoza, H. N. Chui Betancur, and E. Huaquisto Ramos, "Confort térmico y el riesgo de infecciones respiratorias en los adultos mayores en la sierra rural del Perú," *Revista Española de Geriatría y Gerontología*, vol. 56, no. 1, pp. 24–28, Jan. 2021, doi: 10.1016/j.regg.2020.07.007.
3. H. Janssen *et al.*, "Cold indoor temperatures and their association with health and well-being: a systematic literature review," *Public Health*, vol. 224, pp. 185–194, Nov. 2023, doi: 10.1016/j.puhe.2023.09.006.
4. H. Thomson, S. Thomas, E. Sellström, and M. Petticrew, "Housing Improvements for Health and Associated Socio-Economic Outcomes: A Systematic Review," *Campbell Systematic Reviews*, vol. 9, no. 1, pp. 1–348, Jan. 2013, doi: 10.4073/csr.2013.2.
5. H. U. Rehman, M. Hamdy, and A. Hasan, "Towards Extensive Definition and Planning of Energy Resilience in Buildings in Cold Climate," *Buildings*, vol. 14, no. 5, p. 1453, May 2024, doi: 10.3390/buildings14051453.

 doi:10.20944/preprints202602.1796.v1




6. Martín Wieser, Antonio Garaycochea, and Varinia Prada, "Improving the thermal performance of schools in the High Andean Region of Peru. The case of 'PRONIED'S prefabricated frost-type modular classrooms,'" *Revista Hábitat Sustentable*, vol. 13, no. 1, pp. 56–67, June 2023, doi: 10.22320/07190700.2023.13.01.05.
7. I. Miño-Rodríguez, C. Naranjo-Mendoza, and I. Korolija, "Thermal Assessment of Low-Cost Rural Housing—A Case Study in the Ecuadorian Andes," *Buildings*, vol. 6, no. 3, p. 36, Sept. 2016, doi: 10.3390/buildings6030036.
8. J. R. Molina, G. Lefebvre, and M. M. Gómez, "Study of the thermal comfort and the energy required to achieve it for housing modules in the environment of a high Andean rural area in Peru," *Energy and Buildings*, vol. 281, p. 112757, Feb. 2023, doi: 10.1016/j.enbuild.2022.112757.
9. E. Mejia-Solis, J. Arias, and B. Palm, "Simple solutions for improving thermal comfort in huts in the highlands of Peru," *Heliyon*, vol. 9, no. 10, p. e19709, Oct. 2023, doi: 10.1016/j.heliyon.2023.e19709.
10. M. Wieser, S. Rodríguez-Larraín, and S. Onnis, "Estrategias bioclimáticas para clima frío tropical de altura. Validación de prototipo de vivienda. Puno, Perú.," *est*, vol. 10, no. 19, pp. 9–19, Jan. 2021, doi: 10.18537/est.v010.n019.a01.
11. X. Hu, J. Jokisalo, R. Kosonen, M. Lehtonen, and T. Shao, "Cost-Optimal Renovation Solutions for Detached Rural Houses in Severe Cold Regions of China," *Buildings*, vol. 13, no. 3, p. 771, Mar. 2023, doi: 10.3390/buildings13030771.
12. J. R. Molina, J. O. Molina, M. J. Piñas, M. Horn, and M. Gómez, "High Andean bioclimatic dwellings in Peru: climatic conditions, vulnerability of the population and review of academic studies and massification programmes," *Renewable and Sustainable Energy Reviews*, vol. 217, p. 115690, July 2025, doi: 10.1016/j.rser.2025.115690.
13. Anh Tuan Nguyen, A. Nguyen, A. T. Nguyen, Anh Tuan Nguyen, Sigrid Reiter, and S. Reiter, "Passive designs and strategies for low-cost housing using simulation-based optimization and different thermal comfort criteria," *Journal of Building Performance Simulation*, vol. 7, no. 1, pp. 68–81, Jan. 2014, doi: 10.1080/19401493.2013.770067.
14. P. P. F. Da Silva, A. H. Neto, and I. L. Sauer, "Evaluation of Model Calibration Method for Simulation Performance of a Public Hospital in Brazil," *Energies*, vol. 14, no. 13, p. 3791, June 2021, doi: 10.3390/en14133791.
15. Z. Xu, X. Li, B. Sun, Y. Wen, and P. Tang, "Evaluation and Optimization of Traditional Mountain Village Spatial Environment Performance Using Genetic and XGBoost Algorithms in the Early Design Stage—A Case Study in the Cold Regions of China," *Buildings*, vol. 14, no. 9, p. 2796, Sept. 2024, doi: 10.3390/buildings14092796.
16. Y. Duan, T. Zhang, Y. Yang, Y. Wei, Z. Jiao, and W. Gao, "Sensitivity Analysis of Envelope Design for Rural Dwellings in Cold Regions of China: An Orthogonal Experiment-Based Approach," *Buildings*, vol. 15, no. 20, p. 3703, Oct. 2025, doi: 10.3390/buildings15203703.
17. A. Dietz, S. Vera, W. Bustamante, and G. Flamant, "Multi-objective optimization to balance thermal comfort and energy use in a mining camp located in the Andes Mountains at high altitude," *Energy*, vol. 199, p. 117121, May 2020, doi: 10.1016/j.energy.2020.117121.
18. C. Chen *et al.*, "Sensitivity Analysis of Factors Influencing Rural Housing Energy Consumption in Different Household Patterns in the Zhejiang Province," *Buildings*, vol. 13, no. 2, p. 463, Feb. 2023, doi: 10.3390/buildings13020463.
19. Y. Chu, J. Li, and P. Zhao, "Multi-Objective Optimization of Envelope Structures for Rural Dwellings in Qianbei Region, China: Synergistic Enhancement of Energy Efficiency, Thermal Comfort, and Economic Viability," *Buildings*, vol. 15, no. 8, p. 1367, Apr. 2025, doi: 10.3390/buildings15081367.
20. B. Liu, Y. Liu, Q. Xin, X. Kou, and J. Song, "Energy-Efficient Design of Immigrant Resettlement Housing in Qinghai: Solar Energy Utilization, Sunspace Temperature Control, and Envelope Optimization," *Buildings*, vol. 15, no. 9, p. 1434, Apr. 2025, doi: 10.3390/buildings15091434.
21. Q. Yang, F. Xu, W. Lu, Z. Yang, Y. Bai, and B. Wen, "Green renovation and multi-objective optimization of Tibetan courtyard dwellings," *Building and Environment*, vol. 279, p. 113071, July 2025, doi: 10.1016/j.buildenv.2025.113071.

 doi:10.20944/preprints202602.1796.v1




22. C. P. Iruri Ramos, P. Domínguez Gómez, and F. Celis D'amico, "Mejoramiento de la envolvente para el comportamiento térmico de viviendas rurales. Valle del Colca, Perú," *Revista Estoa*, vol. 12, no. 23, pp. 113–124, Jan. 2023, doi: 10.18537/est.v012.n023.a09.
23. C. Yang and A. Misni, "Analysis of Thermal Comfort in Single-Story Courtyard Vernacular Dwellings in Rural China: Passive Design Strategies for Adapting to the Climate," *Buildings*, vol. 15, no. 21, p. 3964, Nov. 2025, doi: 10.3390/buildings15213964.
24. J Rodriguez Molina *et al.*, "Bioclimatic approach for rural dwellings in the cold, high Andean region: A case study of a Peruvian house," *Energy and Buildings*, vol. 231, p. 110605, 2020, doi: 10.1016/j.enbuild.2020.110605.
25. J. M. F. Pardo, "Challenges and Current Research Trends for Vernacular Architecture in a Global World: A Literature Review," *Buildings*, vol. 13, no. 1, p. 162, Jan. 2023, doi: 10.3390/buildings13010162.
26. "Vernacular Passive Strategies for Sustainable Houses in the Andean Ecuadorian Context," in *Lecture Notes in Civil Engineering*, Singapore: Springer Nature Singapore, 2022, pp. 329–336. doi: 10.1007/978-981-16-6932-3_29.
27. J. Torres-Quezada and S. Lituma-Saetama, "Estrategias de sostenibilidad enfocadas al confort térmico y la energia incorporada de una vivienda emergente en la Región Andina del Ecuador," *HS*, vol. 13, no. 1, pp. 42–55, June 2023, doi: 10.22320/07190700.2023.13.01.04.
28. D. K. Pari-Quispe, J. Cronemberger-Ribeiro Silva, S. Huaquisto-Cáceres, H. A. Ccama-Condori, and L. C. Aza-Medina, "Percepción térmica de usuarios en la vivienda vernácula de la comunidad Uro del lago Titicaca en Perú," *HS*, vol. 14, no. 1, pp. 22–33, June 2024, doi: 10.22320/07190700.2024.14.01.02.
29. J. F. Hidalgo-Cordero and L. C. Aza-Medina, "Analysis of the thermal performance of elements made with totora using different production processes," *Journal of Building Engineering*, vol. 65, p. 105777, Apr. 2023, doi: 10.1016/j.jobe.2022.105777.
30. J. Litardo, J. Macías, R. Hidalgo-León, M. G. Cando, and G. Soriano, "Measuring the Effect of Local Commercial Roofing Samples on the Thermal Behavior of a Social Interest Dwelling Located in Different Climates in Ecuador," in *Volume 6: Energy*, Salt Lake City, Utah, USA: American Society of Mechanical Engineers, Nov. 2019, p. V006T06A047. doi: 10.1115/IMECE2019-11472.
31. F. Ordóñez, F. Jácome, P. Castro, and C. Naranjo-Mendoza, "Sensitivity analysis of the variables affecting indoor thermal conditions on unconditioned dwellings in equatorial high-altitude regions from an experimentally validated model," *Advances in Building Energy Research*, vol. 15, no. 4, pp. 442–465, July 2021, doi: 10.1080/17512549.2019.1582437.
32. J. O. Molina Fuertes, M. Ponce, M. H. Mutschler, and M. M. Gómez, "Towards a Sustainable Bioclimatic Approach for the Peruvian High Andean Rural Area: Evaluation of the Thermal Contribution of a Greenhouse Attached to a Dwelling," in *Proceedings of the ISES Solar World Congress 2019*, Santiago, Chile: International Solar Energy Society, 2019, pp. 1–10. doi: 10.18086/swc.2019.08.07.
33. D. E. Okonta, "Investigating the impact of building materials on energy efficiency and indoor cooling in Nigerian homes," *Heliyon*, vol. 9, no. 9, p. e20316, Sept. 2023, doi: 10.1016/j.heliyon.2023.e20316.
34. T. De Rubeis, A. Ciccozzi, D. Paoletti, and D. Ambrosini, "3D printing for energy optimization of building envelope – Experimental results," *Heliyon*, vol. 10, no. 10, p. e31107, May 2024, doi: 10.1016/j.heliyon.2024.e31107.
35. Y. Guo *et al.*, "Thermal comfort and adaptive behaviors in office buildings: A pilot study in Turpan (China) during summer," *Heliyon*, vol. 9, no. 10, p. e20646, Oct. 2023, doi: 10.1016/j.heliyon.2023.e20646.
36. C. M. Calama-González *et al.*, "Thermal insulation impact on overheating vulnerability reduction in Mediterranean dwellings," *Heliyon*, vol. 9, no. 5, p. e16102, May 2023, doi: 10.1016/j.heliyon.2023.e16102.
37. A. Y. Moyou, A. Njifenjou, P. Tiam Kapen, and D. Fokwa, "Numerical computation of heat transfer, moisture transport and thermal comfort through walls of buildings made of concrete material in the city of Douala, Cameroon: An ab initio investigation," *Heliyon*, vol. 10, no. 13, p. e34058, July 2024, doi: 10.1016/j.heliyon.2024.e34058.
38. M. Mangeli, F. Aram, and R. Abouei, "Energy consumption and thermal comfort of rock-cut and modern buildings," *Heliyon*, vol. 10, no. 14, p. e34217, July 2024, doi: 10.1016/j.heliyon.2024.e34217.

 doi:10.20944/preprints202602.1796.v1




39. S. Li *et al.*, "Energy Saving and Thermal Comfort Performance of Passive Retrofitting Measures for Traditional Rammed Earth House in Lingnan, China," *Buildings*, vol. 12, no. 10, p. 1716, Oct. 2022, doi: 10.3390/buildings12101716.
40. E. Delgado-Gutierrez, C. Rubio-Bellido, and J. Canivell, "Thermal Comfort in Social Housing in Ecuador: Do Free-Running Buildings Work in Current and Future Climates?," *Buildings*, vol. 15, no. 12, p. 2018, June 2025, doi: 10.3390/buildings15122018.
41. X. Ma, Z. Mao, and H. Xuan, "Spatial Performance Optimization of High-Altitude Residential Buildings Based on the Thermal Buffer Effect: A Case Study of New-Type Vernacular Housing in Lhasa," *Buildings*, vol. 15, no. 23, p. 4337, Nov. 2025, doi: 10.3390/buildings15234337.
42. T. Shao, W. Zheng, and Z. Cheng, "Passive Energy-Saving Optimal Design for Rural Residences of Hanzhong Region in Northwest China Based on Performance Simulation and Optimization Algorithm," *Buildings*, vol. 11, no. 9, p. 421, Sept. 2021, doi: 10.3390/buildings11090421.
43. E. Mejía-Solís *et al.*, "Evaluating thermal comfort models in high-altitude rural areas of the Peruvian Andes," *RHS*, pp. 36–51, Dec. 2025, doi: 10.22320/07190700.2025.15.02.03.
44. P. Baquedano, R. R. Eudave, F. N. Miranda, S. Graus, and T. M. Ferreira, "Traditional earth construction in Latin America: A review on the construction systems and reinforcement strategies," in *Masonry Construction in Active Seismic Regions*, Elsevier, 2021, pp. 99–121. doi: 10.1016/B978-0-12-821087-1.00011-9.
45. G. Giuffrida, L. Dipasquale, R. M. Pulselli, and R. Caponetto, "Compared Environmental Lifecycle Performances of Earth-Based Walls to Drive Building Envelope Design," *Sustainability*, vol. 16, no. 4, p. 1367, Feb. 2024, doi: 10.3390/su16041367.
46. Drury B. Crawley *et al.*, "EnergyPlus: creating a new-generation building energy simulation program," *Energy and Buildings*, vol. 33, no. 4, pp. 319–331, Apr. 2001, doi: 10.1016/s0378-7788(00)00114-6.
47. ASHRAE, *2021 ASHRAE Handbook - Fundamentals*. Atlanta, GA: American Society of Heating (ASHRAE), 2021.
48. International Organization for Standardization, *Building components and building elements — Thermal resistance and thermal transmittance — Calculation method*, ISO 6946:2017, 2017.
49. E. Mejía-Solís *et al.*, "Evaluating thermal comfort models in high-altitude rural areas of the Peruvian Andes," *RHS*, pp. 36–51, Dec. 2025, doi: 10.22320/07190700.2025.15.02.03.
50. B. L. Capehart, W. J. Kennedy, and W. C. Turner, *Guide to energy management*, Eighth edition, International version. Lilburn, [Georgia]: CRC Press, 2016.
51. *2023 ASHRAE® handbook. HVAC Applications*, SI edition. Atlanta, Ga.: ASHRAE, 2023.
52. OSINERGMIN, "Pliego Tarifario de Electricidad – Electro Sur Este S.A.A," Osinergmin.gob.pe. [Online]. Accessed: Apr. 13, 2025. [Online]. Available: https://www.osinergmin.gob.pe/Tarifas/Electricidad/PliegoTarifario?Id=80000.
53. Y. Deng *et al.*, "Simulation-based sensitivity analysis of energy performance applied to an old Beijing residential neighbourhood for retrofit strategy optimisation with climate change prediction," *Energy and Buildings*, vol. 294, p. 113284, Sept. 2023, doi: 10.1016/j.enbuild.2023.113284.
54. A. Machard *et al.*, "Climate change influence on buildings dynamic thermal behavior during summer overheating periods: An in-depth sensitivity analysis," *Energy and Buildings*, vol. 284, p. 112758, Apr. 2023, doi: 10.1016/j.enbuild.2022.112758.
55. D. Garcia Sanchez, B. Lacarrière, M. Musy, and B. Bourges, "Application of sensitivity analysis in building energy simulations: Combining first- and second-order elementary effects methods," *Energy and Buildings*, vol. 68, pp. 741–750, Jan. 2014, doi: 10.1016/j.enbuild.2012.08.048.
56. A. Saltelli *et al.*, *Global Sensitivity Analysis. The Primer*, 1st ed. Wiley, 2007. doi: 10.1002/9780470725184.
57. M. D. Morris, "Factorial Sampling Plans for Preliminary Computational Experiments," *Technometrics*, vol. 33, no. 2, pp. 161–174, May 1991, doi: 10.1080/00401706.1991.10484804.
58. K. Menberg, Y. Heo, and R. Choudhary, "Sensitivity analysis methods for building energy models: Comparing computational costs and extractable information," *Energy and Buildings*, vol. 133, pp. 433–445, Dec. 2016, doi: 10.1016/j.enbuild.2016.10.005.

 doi:10.20944/preprints202602.1796.v1




59. G. A. Faggianelli, L. Mora, and R. Merheb, "Uncertainty quantification for Energy Savings Performance Contracting: Application to an office building," *Energy and Buildings*, vol. 152, pp. 61–72, Oct. 2017, doi: 10.1016/j.enbuild.2017.07.022.
60. M. H. Kristensen and S. Petersen, "Choosing the appropriate sensitivity analysis method for building energy model-based investigations," *Energy and Buildings*, vol. 130, pp. 166–176, Oct. 2016, doi: 10.1016/j.enbuild.2016.08.038.
61. I. M. Sobol', "Global sensitivity indices for nonlinear mathematical models and their Monte Carlo estimates," *Mathematics and Computers in Simulation*, vol. 55, no. 1–3, pp. 271–280, Feb. 2001, doi: 10.1016/S0378-4754(00)00270-6.
62. Z. Yang and B. Becerik-Gerber, "A model calibration framework for simultaneous multi-level building energy simulation," *Applied Energy*, vol. 149, pp. 415–431, July 2015, doi: 10.1016/j.apenergy.2015.03.048.
63. T. Homma and A. Saltelli, "Importance measures in global sensitivity analysis of nonlinear models," *Reliability Engineering & System Safety*, vol. 52, no. 1, pp. 1–17, Apr. 1996, doi: 10.1016/0951-8320(96)00002-6.
64. L. E. Juanicó and A. D. González, "Thermal insulators with multiple air gaps: Performance, cost and embodied impacts," *Journal of Building Engineering*, vol. 12, pp. 188–195, July 2017, doi: 10.1016/j.jobe.2017.06.005.
65. L. E. Juanicó, "Thermal insulation of roofs by using multiple air gaps separated by insulating layers of low infrared emissivity," *Construction and Building Materials*, vol. 230, p. 116931, Jan. 2020, doi: 10.1016/j.conbuildmat.2019.116931.
66. Rahul Verma and Dibakar Rakshit, "Comparison of reflective coating with other passive strategies: A climate based design and optimization study of building envelope," *Energy and Buildings*, vol. 287, pp. 112973–112973, May 2023, doi: 10.1016/j.enbuild.2023.112973.
67. Letiane Benincá, Eva Crespo Sánchez, Ana Passuello, Rodrigo Karini Leitzke, Eduardo Grala da Cunha, and José Maria González Barroso, "Multi-objective optimization of the solar orientation of two residential multifamily buildings in south Brazil," vol. 285, pp. 112838–112838, Apr. 2023, doi: 10.1016/j.enbuild.2023.112838.
68. D. E. Goldberg and D. E. Goldberg, *Genetic algorithms in search, optimization, and machine learning*, 30. print. Boston: Addison-Wesley, 2012.
69. L. A. Scardua, *Applied evolutionary algorithms for engineers using Python*. in A Science Publishers book. Boca Raton: CRC Press, 2021.